Biologically Inspired Swimming Snake Robots: Modeling, Control and Experimental Investigation

Eleni Kelasidi, *Member, IEEE,* Pål Liljebäck, *Member, IEEE,* Kristin Y. Pettersen, *Senior Member, IEEE,* and Jan Tommy Gravdahl, *Senior Member, IEEE*

***Abstract*—Increasing efficiency by improving locomotion methods is a key issue for underwater robots. Moreover, a number of different control design challenges must be solved in order to realize operational swimming robots for underwater tasks. This paper proposes and experimentally validates a straight line path following controller for biologically inspired swimming snake robots. In particular, a line-of-sight (LOS) guidance law is presented, which is combined with a sinusoidal gait pattern and a directional controller that steers the robot towards and along the desired path. The performance of the path following controller is investigated through experiments with a physical underwater snake robot for both lateral undulation and eel-like motion. In addition, fluid parameter identification is performed and simulation results based on the identified fluid coefficients are presented to obtain back-to-back comparison with the motion of the physical robot during the experiments. The experimental results show that the proposed control strategy successfully steers the robot towards and along the desired path for both lateral undulation and eel-like motion patterns.**

***Index Terms*—Underwater snake robots, modeling of swimming robots, model identification, LOS path following controller.**

I. Introduction

THE use of robotic underwater vehicles has rapidly increased during the last decades due to technological innovations which enable these mechanisms to operate in deep and harsh subsea environments. Nowadays, autonomous underwater vehicles (AUVs) and remotely operated vehicles (ROVs) are widely used subsea for different challenging tasks [1], such as inspection, surveillance, maintenance, repair, and construction, and they are extensively used in the subsea oil and gas industry and by the science community. In addition, swimming snake robots represent an interesting alternative to conventional ROVs and AUVs.

For centuries, engineers and scientists have gained inspiration from the natural world in their search for solutions to technical problems, a process termed biomimetics. To this end, inspired by biological swimming creatures, underwater snake robots carry the potential of meeting the growing need for robotic mobility in underwater environments. These mechanisms have a long, slender and flexible body which enable them to reach and operate in locations not accessible by larger and more conventional underwater vehicles. At the same time, a swimming snake robot carries manipulation capabilities as an inherent part of its body since it is essentially a mobile manipulator arm. Underwater snake robots thus bring a promising prospective to improve the efficiency and maneuverability of modern-day underwater vehicles. A particularly relevant application concerns inspection and maintenance of subsea oil and gas installations, where the ability to reach tight locations in between pipe structures is important. Moreover, for the biological community and marine archeology, snake robots that can swim smoothly with limited noise, and that can navigate in difficult environments such as ship wrecks, are very interesting [2]. To realize operational snake robots for such underwater applications, a number of different control design challenges must first be solved. An important control problem concerns the ability to follow given reference paths, and this is the topic of this paper.

Studies of biologically inspired snake robots have largely restricted themselves to land-based studies for which reviews on modelling, implementation, and control of snake robots have been presented in [3]–[5]. Empirical and analytic studies of snake locomotion were reported by [6], while the work of [7] is among the first approaches to develop a snake robot prototype. Several land-based snake robots [8]–[10] and biologically inspired swimming robots [11]–[19] have been constructed since then. Due to the complex dynamics of swimming snake robots, several different modeling approaches have been carried out in the literature [2], [14], [20]–[28]. Several results have been reported in the related field of design, modeling and control of underwater robots that mimic the movement of fish [18], [19], [29]–[32]. In addition, sandfish lizard locomotion has been studied as inspiration for a robot design in [33]. A comparison of these approaches is presented in [34].

Most modeling approaches for underwater snake robots omit the fluid moments (fluid torques) by considering that their effect on the motion of the robot is negligible [22], [26], [35]. However, including the impact of the fluid torques on the power consumption of the system (see e.g. [25]), will improve the accuracy of the model from a hydrodynamic and energy efficiency point of view. The works in [23], [25] and [36] propose the modeling of fluid torques, with the drag force and torque evaluated numerically. These approaches lack a closed form solution, which is a drawback since a hydrodynamic model in closed form is advantageous for model-based analysis and control design. The works in [2], [37] present a closed form hydrodynamic model, where hydrodynamic forces and torques are considered and where there is no need for algorithmic computations of drag effects. Furthermore, in this

E. Kelasidi, and K. Y. Pettersen are with the Centre for Autonomous Marine Operations and Systems, Dept. of Engineering Cybernetics at NTNU, NO-7491 Trondheim, Norway. E-mail: {Eleni.Kelasidi,Kristin.Y.Pettersen}@itk.ntnu.no

P. Liljebäck and J. T. Gravdahl are with the Dept. of Engineering Cybernetics at NTNU, NO-7491 Trondheim, Norway. E-mail: {Pal.Liljeback,Tommy.Gravdahl}@itk.ntnu.no

This work was partly supported by the Research Council of Norway through project no. 205622 and its Centres of Excellence funding scheme, project no. 223254-AMOS

This paper has supplementary downloadable material available at http://ieeexplore.ieee.org, provided by the authors. This includes three-multimedia wmv format movie clips, which show experimental results carried out with a biologically inspired underwater snake robot. This material is 40 MB in size.

approach, both linear and nonlinear drag forces (resistive fluid forces), the added mass effect (reactive fluid forces), the fluid moments, and current effects are considered. The resulting closed form model is well suited for model-based control design schemes. In this paper, the adopted control design will be based on the model presented in [2], [37].

Previous control approaches for underwater snake robots proposed in the literature have mainly been concerned with forward and turning locomotion [14], [38]. Thus, the next step would be path following control. To this end, [22], [39] and [18] propose controllers for tracking straight and curved trajectories based on synthesizing gaits for translational and rotational motion of various fish-like mechanisms. The evolution from fish to amphibian using the same concept is presented in [13] by employing central pattern generators (CPG). Moreover, [22] and [40] propose controllers for tracking straight and curved trajectories for eel-like motion. In [41], the path to be followed by the underwater snake robot is defined by straight lines of interconnected points, combining an artificial potential field-based path planner with a new waypoint guidance strategy. A different waypoint guidance strategy is described in [42] for a carangiform swimmer, having the waypoints defined a priori.

Several previous works consider control schemes for eel-like robot locomotion. In particular, [43] develops a feedback control scheme for 3D movement of the robot's continuous model presented in [23]. In [44], motion control of a three-dimensional eel-like robot without pectoral fins is described, while in [45] a multi-variable constrained feedback control scheme is proposed, considering a reduced model of an eel robot. A methodology for path following of eel-like robots is presented in [46] based on autonomous gait generation extracted from the controlled local system curvature. Open-loop motion planning for eel-like robots is presented in [22], [38] and [14], including the experimental evaluation of the adopted techniques. Furthermore, in [22], experiments for closed-loop straight line tracking using image-based position feedback are implemented with disturbance rejection in the plane. Nevertheless, these preliminary experiments were not satisfactory, as mentioned by the authors [22], although proving the general concept. In [34], an underwater snake robot is commanded to track a straight line path in the presence of ocean currents of unknown direction and magnitude, controlled by an integral line-of-sight (LOS) path following controller. The presented experimental results confirmed that the proposed integral LOS guidance law can be applied to underwater snake robots to achieve not only tracking of straight lines, but also to compensate for ocean drift effects, including current effects.

Another important control problem for underwater vehicles concerns the ability to achieve efficient motion with preferably a minimum amount of consumed energy in order to be able to undertake longer missions. Hence, for the long term autonomy of underwater vehicles, energy efficiency is one of the main challenges. Solutions in this direction are proposed in [47], [48]. In particular, in [47], the relationships between the parameters of the gait patterns, the consumed energy, and the forward velocity for different motion patterns for underwater snake robots were investigated. In addition, empirical rules were proposed in order to choose the most efficient motion pattern. In [48], a simulation study was undertaken in order to compare the power consumption of swimming snake robots with that of today's benchmark solution for subsea inspection, maintenance and repair, which are ROVs. The presented simulation results showed that, with respect to the cost of transportation metric and the total consumed energy, the underwater snake robots are more energy efficient than an ROV for all the compared motion modes.

This paper considers path following control of swimming snake robots. Based on the dynamic model presented in [2], [37], we formulate a line-of-sight path following controller for steering an underwater snake robot along a straight line path. The LOS guidance law is inspired by path following control of marine surface vessels [1], which is widely used for directional control of these vessels. A preliminary investigation of the control strategy was presented in [41], but whereas the efficacy of the control strategy is supported by simulation results in [41], this paper investigates its efficacy through experiments with a physical underwater snake robot [17].

The first contribution of this paper are experimental results which show that the LOS guidance law can be applied to underwater snake robots to achieve straight line path following for both lateral undulation and eel-like motion patterns. This contribution extends our previous work in [34], where a less extensive experimental study was carried out for the case of lateral undulation motion only. Lateral undulation and eel-like motion are both highly relevant motion patterns for underwater snake robots. An experimental study considering both motion patterns is therefore interesting since it allows the two motion patterns to be compared.

The second contribution of this paper is a comparative study between the experimental results and the corresponding simulation results. In particuar, the experimental results are compared with simulation results that are obtained after carrying out fluid parameter identification of the model presented in [2], [37]. Whereas the simulation study in [41] was carried out by considering theoretical values for the fluid parameters, this paper presents preliminary experimental results obtained for the fluid coefficients using a physical underwater snake robot [17], thereby allowing us to obtain an accurate back-to-back comparison of real experimental and simulated data. This gives us the opportunity to obtain not only qualitative comparison results as in [34] and [41], but also a quantitative comparison between the motion of the simulated and the physical snake robot.

In [14], simulation results of a fish-like robot with caudal tail named AmphiBot III were obtained via numerical integration in real time and compared with experimental results by calibrating the fluid coefficients. By using the large amplitude elongated body theory (LAEBT) [14] also considers the reaction force exerted on the caudal fin in conjunction with swimming locomotion. In this paper, however, we assume a cylindrical shape for all links including the tail, so that an explicit tail model is not considered. Furthermore, we present preliminary results for the fluid coefficients identification for the model presented in [2], [37]. To the authors' best knowledge, experimental validation of a complex fluid model that takes into account both the reactive (added mass effects) and resistive forces (combination of linear and nonlinear drag forces), while being expressed in closed form have not been investigated in previous literature. Moreover, in this paper we propose a solution for path following of underwater snake robots supported by simulation and experimental results. Experimental results show that the snake robot is able to follow the reference path both for lateral undulation and eel-like

motion, and using the results presented in [47], [48] regarding the power efficiency of the underwater snake robots, we can argue that underwater swimming robots can be considered as good candidates for different challenging tasks in the subsea environment.

The paper is organized as follows. Section II presents the dynamic model of an underwater snake robot, while the line-of-sight (LOS) path following controller is outlined in Section III. The experimental setup is presented in Section IV, followed by the fluid parameters identification approach in Section V. Experimental and simulation results for the proposed path following control strategy are presented both for lateral undulation and eel-like motion in Section VI. Finally, conclusions and suggestions for further research are given in Section VII.

II. Mathematical Model of Underwater Snake Robot

This section briefly presents a model of the kinematics and dynamics of an underwater snake robot moving in a virtual horizontal plane, that will be used in the control design and analysis of this paper. A more detailed presentation of the model can be found in [2], [37].

A. Notations and Defined Symbols

The underwater snake robot consists of n rigid links of equal length $2l$ interconnected by $n-1$ joints. The links are assumed to have the same mass m and moment of inertia $J = \frac{1}{3}ml^2$. The mass of each link is uniformly distributed so that the link CM (center of mass) is located at its center point (at length l from the joint at each side). The total mass of the snake robot is therefore nm. In the following subsections, the kinematics and dynamics of the robot will be described in terms of the mathematical symbols described in Table I and illustrated in Fig. 1 and Fig. 2. The following vectors and matrices are used in the subsequent sections:

$$\mathbf{A} = \begin{bmatrix} 1 & 1 & & \\ & \ddots & \ddots & \\ & & 1 & 1 \end{bmatrix}, \mathbf{D} = \begin{bmatrix} 1 & -1 & & \\ & \ddots & \ddots & \\ & & 1 & -1 \end{bmatrix},$$

where $\mathbf{A}, \mathbf{D} \in \mathbb{R}^{(n-1)\times n}$. Furthermore,

$$\mathbf{e} = \begin{bmatrix} 1 & \dots & 1 \end{bmatrix}^T \in \mathbb{R}^n, \mathbf{E} = \begin{bmatrix} \mathbf{e} & \mathbf{0}_{n\times 1} \\ \mathbf{0}_{n\times 1} & \mathbf{e} \end{bmatrix} \in \mathbb{R}^{2n\times 2},$$

$$\mathbf{S}_\theta = \text{diag}(\sin\boldsymbol{\theta}) \in \mathbb{R}^{n\times n}, \quad \mathbf{C}_\theta = \text{diag}(\cos\boldsymbol{\theta}) \in \mathbb{R}^{n\times n}$$

$$\dot{\boldsymbol{\theta}}^2 = \begin{bmatrix} \dot{\theta}_1^{\,2} & \dots & \dot{\theta}_n^{\,2} \end{bmatrix}^T \in \mathbb{R}^n, \mathbf{K} = \mathbf{A}^T\left(\mathbf{D}\mathbf{D}^T\right)^{-1}\mathbf{D}$$

The matrices $\mathbf{A}$ and $\mathbf{D}$ represent, respectively, an addition and a difference matrix, which will be used, for adding and subtracting pairs of adjacent elements of a vector. Furthermore, the vector $\mathbf{e}$ represents a summation vector, which is used for adding all elements of a n-dimensional vector.

B. Kinematics of Underwater Snake Robot

The snake robot is assumed to move in a virtual horizontal plane, fully immersed in water, and has n+2 degrees of freedom (n links angles and the x-y position of the robot). The *link angle* of each link $i \in 1,\dots,n$ of the snake robot is denoted by $\theta_i \in \mathbb{R}$, while the *joint angle* of joint $i \in 1,\dots,n-1$ is given by

$$\phi_i = \theta_i - \theta_{i-1}. \tag{1}$$

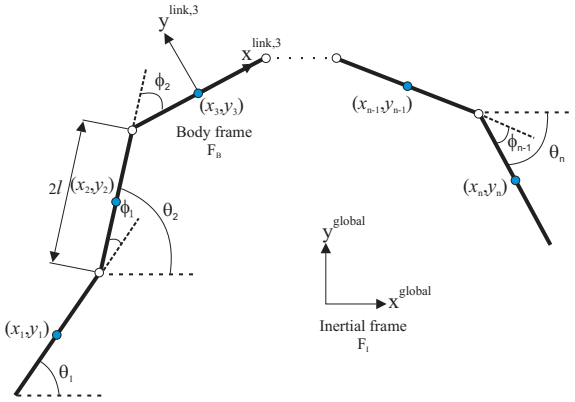

Fig. 1. Kinematic parameters of the underwater snake robot.

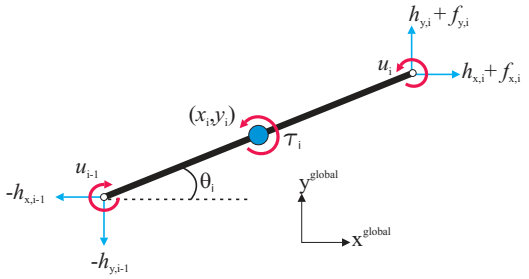

Fig. 2. Forces and torques acting on each link of the underwater snake robot.

The link angles and the joint angles are assembled in the vectors $\boldsymbol{\theta} = [\theta_1,\dots,\theta_n]^T \in \mathbb{R}^n$ and $\boldsymbol{\phi} = [\phi_1,\dots,\phi_{n-1}]^T \in \mathbb{R}^{n-1}$, respectively. The *heading* (or *orientation*) $\bar{\theta} \in \mathbb{R}$ of the snake is defined as the average of the link angles, i.e. as [3]

$$\bar{\theta} = \frac{1}{n}\sum_{i=1}^{n}\theta_i. \tag{2}$$

TABLE I
Definition of Mathematical Terms

Symbol	Description	Vector
n	The number of links	
l	The half length of a link	
m	Mass of each link	
J	Moment of inertia of each link	
θ_i	Angle between link i and the global x axis	$\boldsymbol{\theta} \in \mathbb{R}^n$
ϕ_i	Angle of joint i	$\boldsymbol{\phi} \in \mathbb{R}^{n-1}$
(x_i, y_i)	Global coordinates of the CM of link i	$\mathbf{X}, \mathbf{Y} \in \mathbb{R}^n$
(p_x, p_y)	Global coordinates of the CM of the robot	$\mathbf{p}_{\text{CM}} \in \mathbb{R}^2$
u_i	Actuator torque of joint between link i and link $i+1$	$\mathbf{u} \in \mathbb{R}^{n-1}$
u_{i-1}	Actuator torque of joint between link i and link $i-1$	$\mathbf{u} \in \mathbb{R}^{n-1}$
$f_{x,i}$	Fluid force on link i in x direction	$\mathbf{f_x} \in \mathbb{R}^n$
$f_{y,i}$	Fluid force on link i in y direction	$\mathbf{f_y} \in \mathbb{R}^n$
τ_i	Fluid torque on link i	$\boldsymbol{\tau} \in \mathbb{R}^n$
$h_{x,i}$	Joint constraint force in x direction on link i from link $i+1$	$\mathbf{h_x} \in \mathbb{R}^{n-1}$
$h_{y,i}$	Joint constraint force in y direction on link i from link $i+1$	$\mathbf{h_y} \in \mathbb{R}^{n-1}$
$h_{x,i-1}$	Joint constraint force in x direction on link i from link $i-1$	$\mathbf{h_x} \in \mathbb{R}^{n-1}$
$h_{y,i-1}$	Joint constraint force in y direction on link i from link $i-1$	$\mathbf{h_y} \in \mathbb{R}^{n-1}$

The global frame position $\mathbf{p}_{\text{CM}} \in \mathbb{R}^2$ of the CM (center of mass) of the robot is given by

$$\mathbf{p}_{\text{CM}} = \begin{bmatrix} p_x \\ p_y \end{bmatrix} = \begin{bmatrix} \frac{1}{nm}\sum_{i=1}^{n} m x_i \\ \frac{1}{nm}\sum_{i=1}^{n} m y_i \end{bmatrix} = \frac{1}{n}\begin{bmatrix} \mathbf{e}^T\mathbf{X} \\ \mathbf{e}^T\mathbf{Y} \end{bmatrix}, \quad (3)$$

where (x_i, y_i) are the global frame coordinates of the CM of link i, $\mathbf{X} = [x_1, \ldots, x_n]^T \in \mathbb{R}^n$ and $\mathbf{Y} = [y_1, \ldots, y_n]^T \in \mathbb{R}^n$. The forward velocity of the robot is denoted by $\bar{v}_t \in \mathbb{R}$ and is defined as the component of the CM velocity along the current heading of the snake, i.e.

$$\bar{v}_t = \dot{p}_x \cos\bar{\theta} + \dot{p}_y \sin\bar{\theta}. \quad (4)$$

C. Hydrodynamic Modeling

As it has been noted in the bio-robotics community, underwater snake (eel-like) robots bring a promising prospective to improve the efficiency and maneuverability of modern-day underwater vehicles. The dynamic modeling of the contact forces is, however, quite complicated compared to the modeling of the overall rigid motion. The Navier-Stokes equations are very difficult to solve and quite unsuited for robotics control design purposes. The hydrodynamic modeling approach from [2] that is considered in this paper, takes into account both the linear and the nonlinear drag forces (resistive fluid forces), the added mass effect (reactive fluid forces), the fluid moments and current effects.

In [2], it is shown that the fluid forces on all links can be expressed in vector form as

$$\mathbf{f} = \begin{bmatrix} \mathbf{f_x} \\ \mathbf{f_y} \end{bmatrix} = \begin{bmatrix} \mathbf{f_{A_x}} \\ \mathbf{f_{A_y}} \end{bmatrix} + \begin{bmatrix} \mathbf{f}^{\text{I}}_{\mathbf{D_x}} \\ \mathbf{f}^{\text{I}}_{\mathbf{D_y}} \end{bmatrix} + \begin{bmatrix} \mathbf{f}^{\text{II}}_{\mathbf{D_x}} \\ \mathbf{f}^{\text{II}}_{\mathbf{D_y}} \end{bmatrix}. \quad (5)$$

The vectors $\mathbf{f_{A_x}}$ and $\mathbf{f_{A_y}}$ represent the effects from added mass forces and are expressed as

$$\begin{aligned} \begin{bmatrix} \mathbf{f_{A_x}} \\ \mathbf{f_{A_y}} \end{bmatrix} = &- \begin{bmatrix} \mu_n(\mathbf{S}_\theta)^2 & -\mu_n\mathbf{S}_\theta\mathbf{C}_\theta \\ -\mu_n\mathbf{S}_\theta\mathbf{C}_\theta & \mu_n(\mathbf{C}_\theta)^2 \end{bmatrix} \begin{bmatrix} \ddot{\mathbf{X}} \\ \ddot{\mathbf{Y}} \end{bmatrix} \\ &- \begin{bmatrix} -\mu_n\mathbf{S}_\theta\mathbf{C}_\theta & -\mu_n(\mathbf{S}_\theta)^2 \\ \mu_n(\mathbf{C}_\theta)^2 & \mu_n\mathbf{S}_\theta\mathbf{C}_\theta \end{bmatrix} \begin{bmatrix} \mathbf{V}_x^a \\ \mathbf{V}_y^a \end{bmatrix} \dot{\boldsymbol{\theta}}, \end{aligned} \quad (6)$$

where $\mathbf{V}_x^a = \text{diag}(V_{x,1}, \ldots, V_{x,n}) \in \mathbb{R}^{n\times n}$, $\mathbf{V}_y^a = \text{diag}(V_{y,1}, \ldots, V_{y,n}) \in \mathbb{R}^{n\times n}$ and $[V_{x,i}, V_{y,i}]^T$ is the current velocity expressed in inertial frame coordinates. The drag forces on the robot are given by

$$\begin{bmatrix} \mathbf{f}^{\text{I}}_{\mathbf{D_x}} \\ \mathbf{f}^{\text{I}}_{\mathbf{D_y}} \end{bmatrix} = - \begin{bmatrix} c_t\mathbf{C}_\theta & -c_n\mathbf{S}_\theta \\ c_t\mathbf{S}_\theta & c_n\mathbf{C}_\theta \end{bmatrix} \begin{bmatrix} \mathbf{V_{r_x}} \\ \mathbf{V_{r_y}} \end{bmatrix}, \quad (7)$$

$$\begin{bmatrix} \mathbf{f}^{\text{II}}_{\mathbf{D_x}} \\ \mathbf{f}^{\text{II}}_{\mathbf{D_y}} \end{bmatrix} = - \begin{bmatrix} c_t\mathbf{C}_\theta & -c_n\mathbf{S}_\theta \\ c_t\mathbf{S}_\theta & c_n\mathbf{C}_\theta \end{bmatrix} \text{sgn}\left(\begin{bmatrix} \mathbf{V_{r_x}} \\ \mathbf{V_{r_y}} \end{bmatrix} \right) \begin{bmatrix} \mathbf{V_{r_x}}^2 \\ \mathbf{V_{r_y}}^2 \end{bmatrix}, \quad (8)$$

where $\mathbf{f}^{\text{I}}_{\mathbf{D_x}}$, $\mathbf{f}^{\text{I}}_{\mathbf{D_y}}$ and $\mathbf{f}^{\text{II}}_{\mathbf{D_x}}$, $\mathbf{f}^{\text{II}}_{\mathbf{D_y}}$ are the linear and nonlinear drag forces, respectively, and where the relative link velocities $\mathbf{V_{r_x}}$ and $\mathbf{V_{r_y}}$ are given by

$$\begin{bmatrix} \mathbf{V_{r_x}} \\ \mathbf{V_{r_y}} \end{bmatrix} = \begin{bmatrix} \mathbf{C}_\theta & \mathbf{S}_\theta \\ -\mathbf{S}_\theta & \mathbf{C}_\theta \end{bmatrix} \begin{bmatrix} \dot{\mathbf{X}} - \mathbf{V}_x \\ \dot{\mathbf{Y}} - \mathbf{V}_y \end{bmatrix}. \quad (9)$$

In addition, the fluid torques on all links are

$$\boldsymbol{\tau} = -\boldsymbol{\Lambda}_1\ddot{\boldsymbol{\theta}} - \boldsymbol{\Lambda}_2\dot{\boldsymbol{\theta}} - \boldsymbol{\Lambda}_3\dot{\boldsymbol{\theta}}|\dot{\boldsymbol{\theta}}|, \quad (10)$$

where $\boldsymbol{\Lambda}_1 = \lambda_1\mathbf{I}_n$, $\boldsymbol{\Lambda}_2 = \lambda_2\mathbf{I}_n$ and $\boldsymbol{\Lambda}_3 = \lambda_3\mathbf{I}_n$. The coefficients c_t, c_n, λ_2, λ_3 represent the drag forces parameters due to the pressure difference between the two sides of the body, and the parameters μ_n, λ_1 represent the added mass of the fluid carried by the moving body. Note that the added mass parameter in the x direction is considered equal to zero ($\mu_t = 0$), because the added mass of a slender body in the longitudinal direction can be neglected compared to the body mass [2].

D. Equations of Motion

This section presents the equations of motion for the underwater snake robot. In [2], [37] it is shown that the acceleration of the CM may be expressed as

$$\begin{aligned} \begin{bmatrix} \ddot{p}_x \\ \ddot{p}_y \end{bmatrix} = &-\mathbf{M}_p \begin{bmatrix} \mathbf{k}_{11} & \mathbf{k}_{12} \\ \mathbf{k}_{21} & \mathbf{k}_{22} \end{bmatrix} \begin{bmatrix} l\mathbf{K}^T(\mathbf{C}_\theta\dot{\boldsymbol{\theta}}^2 + \mathbf{S}_\theta\ddot{\boldsymbol{\theta}}) \\ l\mathbf{K}^T(\mathbf{S}_\theta\dot{\boldsymbol{\theta}}^2 - \mathbf{C}_\theta\ddot{\boldsymbol{\theta}}) \end{bmatrix} \\ &- \mathbf{M}_p \begin{bmatrix} \mathbf{k}_{12} & -\mathbf{k}_{11} \\ \mathbf{k}_{22} & -\mathbf{k}_{21} \end{bmatrix} \begin{bmatrix} \mathbf{V}_x^a \\ \mathbf{V}_y^a \end{bmatrix} \dot{\boldsymbol{\theta}} + \mathbf{M}_p \begin{bmatrix} \mathbf{e}^T\mathbf{f_{Dx}} \\ \mathbf{e}^T\mathbf{f_{Dy}} \end{bmatrix}, \end{aligned} \quad (11)$$

where the detailed derivation of the matrix $\mathbf{M}_p$ and vectors $\mathbf{k}_{11}$, $\mathbf{k}_{12}$, $\mathbf{k}_{21}$ and $\mathbf{k}_{22}$ are given in [2], [37]. In addition, it is shown that under the influence of fluid forces (5) and torques (10), the complete equations of motion of the underwater snake robot are obtained by (11) and

$$\mathbf{M}_{\boldsymbol{\theta}}\ddot{\boldsymbol{\theta}} + \mathbf{W}_{\boldsymbol{\theta}}\dot{\boldsymbol{\theta}}^2 + \mathbf{V}_\theta\dot{\boldsymbol{\theta}} + \boldsymbol{\Lambda}_3|\dot{\boldsymbol{\theta}}|\dot{\boldsymbol{\theta}} + \mathbf{K_{Dx}}\mathbf{f_{Dx}} + \mathbf{K_{Dy}}\mathbf{f_{Dy}} = \mathbf{D}^T\mathbf{u}, \quad (12)$$

with $\mathbf{f_{Dx}} = \mathbf{f}^{\text{I}}_{\mathbf{D_x}} + \mathbf{f}^{\text{II}}_{\mathbf{D_x}}$ and $\mathbf{f_{Dy}} = \mathbf{f}^{\text{I}}_{\mathbf{D_y}} + \mathbf{f}^{\text{II}}_{\mathbf{D_y}}$ representing the drag forces in x and y directions and $\mathbf{u} \in \mathbb{R}^{n-1}$ the control input. For more details and the derivation of the matrices $\mathbf{M}_\theta$, $\mathbf{W}_\theta$, $\mathbf{V}_\theta$, $\mathbf{K_{Dx}}$ and $\mathbf{K_{Dy}}$, see [37].

By introducing the state variable $\mathbf{x} = \left[\boldsymbol{\theta}^T, \mathbf{p}_{\text{CM}}^T, \dot{\boldsymbol{\theta}}^T, \dot{\mathbf{p}}_{\text{CM}}^T\right]^T \in \mathbb{R}^{2n+4}$, we can rewrite the model of the robot compactly in state space form as

$$\dot{\mathbf{x}} = \left[\dot{\boldsymbol{\theta}}^T, \dot{\mathbf{p}}_{\text{CM}}^T, \ddot{\boldsymbol{\theta}}^T, \ddot{\mathbf{p}}_{\text{CM}}^T\right]^T = \mathbf{F}(\mathbf{x}, \mathbf{u}) \quad (13)$$

where the elements of $\mathbf{F}(\mathbf{x}, \mathbf{u})$ are found by solving (11) and (12) for $\ddot{\mathbf{p}}_{\text{CM}}$ and $\ddot{\boldsymbol{\theta}}$, respectively.

Remark 1. It is interesting to note that if, in the dynamic model (11) and (12), we set the fluid parameters to zero and replace the drag forces in the x and y direction with ground friction models [3], then the model reduces exactly to the dynamic model of a ground snake robot described in [3]. The underwater snake robot model is thus an extension of the land snake robot model, and may be used for amphibious snake robots moving both on land and in water.

E. Control Objective

III. LOS Path Following Control

In this section, we present a LOS path following control scheme for underwater snake robots moving in a virtual horizontal plane [41], based on the general sinusoidal motion pattern proposed in [49]. In particular, a function to describe a quite general class of sinusoidal motion patterns suitable for locomotion of underwater snake robots was derived in [49], and is briefly presented in Section III.B.

The structure of the LOS path following controller, as shown in Fig. 3, consists of two parts, the inner-loop PD controller that is used to control the joint angles ϕ and the outer-loop

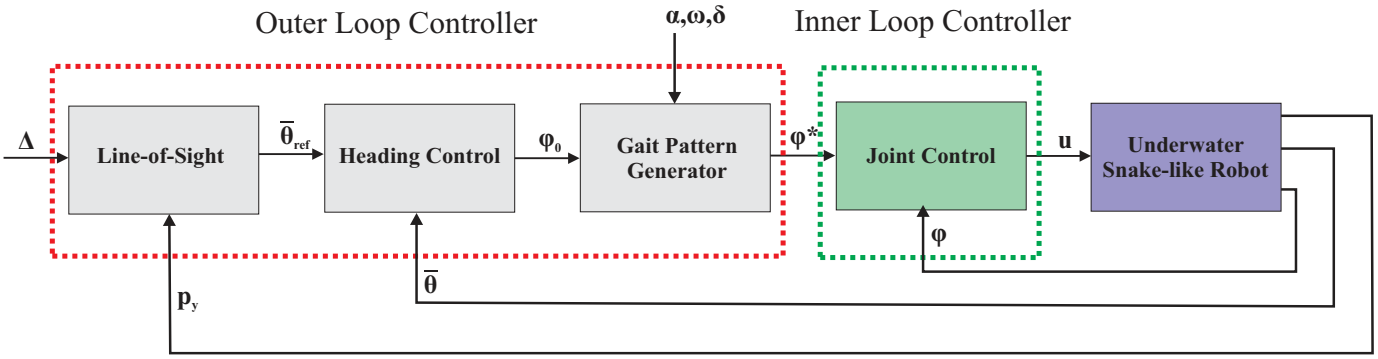

Fig. 3. The structure of the LOS path following controller.

controller that is used for generating the reference joint angles, in order to achieve the desired sinusoidal gait pattern and the desired heading $\bar{\theta}_{\text{ref}}$. The latter controller is composed of three separate components, the gait pattern generator which extracts the sinusoidal motion pattern to propel the robot forward, the heading controller, which steers the robot towards and subsequently along the desired path and the LOS guidance law (Fig. 4), which generates the desired heading angle, in order to reach and follow the desired path. These three components of the path following controller will be presented in the following subsections.

The main control objective is the convergence of the robot to the desired straight line path. The forward velocity $\bar{v}_t$ of the robot, defined in (4), does not require accurate control, but only $\bar{v}_t > 0$ to ensure a nonzero forward velocity for the robot. Regarding the position of the robot in the 2D plane, the desired path is aligned with the global x axis for simplicity, and thus the cross track error along the desired path coincides with the robot's position over the global y axis. Note that the controller can easily be generalized to follow a straight line in any direction by redefining the global x axis with a proper rotational transformation. Furthermore, the heading of the robot (2) corresponds to the angle formed between the robots body and the desired straight line path (Fig. 4). Considering these objectives, the control system can be formalized as

$$\lim_{t\to\infty} p_y = 0 \tag{14}$$

$$\lim_{t\to\infty} \bar{\theta} = 0 \tag{15}$$

$$\lim_{t\to\infty} \bar{v}_t > 0 \tag{16}$$

Note that, since underwater snake robots have an oscillatory gait pattern, the control objectives imply that p_y and $\bar{\theta}$ should have steady state oscillations about zero.

Remark 2. As we have already mentioned, in this paper forward speed control has not been considered. However, in [47] based on extensive simulation results we showed how it is possible to achieve a desired forward velocity for underwater snake robots by simply choosing a proper set for the gait parameters α, ω and δ. In the future, a formal control approach for speed control should be investigated.

A. Motion Pattern

Previous studies on swimming snake robots have focused on two motion patterns; lateral undulation and eel-like motion. In the present study, the adopted motion pattern is a more general sinusoidal motion pattern, which represents a broader class including the aforementioned ones. Lateral undulation [3] constitutes the fastest and most common type of ground snake locomotion. It is achieved by means of body waves, with a constant amplitude, propagated from head to tail, while the snake robot is commanded to follow the serpenoid curve [7]. On the other hand, eel-like motion can be achieved by propagating lateral axial undulations with increasing amplitude from head to tail [29]. To achieve the general sinusoidal motion pattern, each joint $i \in \{1, \cdots, n-1\}$ of the underwater snake robot is commanded to track the reference signal

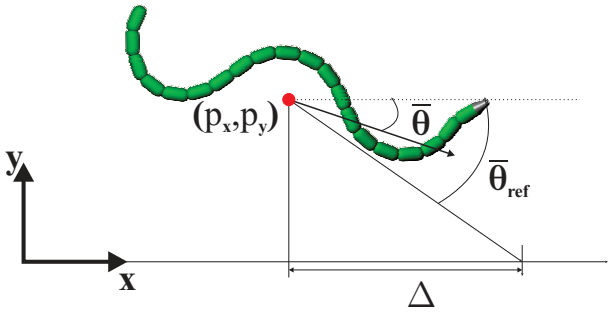

Fig. 4. Illustration of the LOS guidance law.

$$\phi_i^*(t) = \alpha \mathrm{g}(i,n) \sin(\omega t + (i-1)\delta) + \phi_0, \tag{17}$$

where α and ω are the maximum amplitude and the frequency, respectively, δ determines the phase shift between the joints, while the function $\mathrm{g}(i,n)$ is a scaling function for the amplitude of joint i [49]. This scaling function allows (17) to describe a quite general class of sinusoidal functions, including several different snake motion patterns. For instance, $\mathrm{g}(i,n) = 1$ gives lateral undulation, while $\mathrm{g}(i,n) = (n-i)/(n+1)$ gives eel-like motion [2]. Finally, the parameter ϕ_0 is a joint offset coordinate that is shown to affect the direction of locomotion in the case of land-based snake robots [3] and fish robots [42] as well. In this paper, the joint offset will be used in order to control the direction of the locomotion of underwater snake robots.

B. Outer-Loop Controller

As noted above, the outer-loop controller generates the reference joint angles, in order to achieve the desired sinusoidal gait pattern and the desired orientation for the robot. Regarding the sinusoidal gait pattern, previous approaches

keep the parameters α and δ fixed, while ω, ϕ_0 are used to control the speed and the direction of the snake robot, respectively, [3], [42], [50]. In this paper, the same approach will be adopted. The orientation $\bar{\theta}$ of the robot is given by (2). Moreover, for the desired orientation, motivated by [51], [1], we propose to define the reference orientation using the following LOS guidance law

$$\bar{\theta}_{\text{ref}} = -\arctan\left(\frac{p_y}{\Delta}\right), \qquad \Delta > 0 \tag{18}$$

where p_y is the cross-track error (i.e., the position of the underwater snake robot along the global y axis), while Δ is a constant design parameter. In particular, Δ denotes the *look-ahead distance* that influences the rate of convergence to the desired path [1]. Note that LOS guidance laws are much used in practice for path following control of marine surface vessels [1], [52] and have been used for path following control of ground snake robots [3].

Remark 3. The *look-ahead distance* Δ is a fundamental parameter for the LOS guidance law since this parameter directly affects the transient motion of the underwater snake robot. A large value of Δ results in a well-damped transient motion, but the convergence to the desired path becomes slow, cf. Fig. 4. In contrast, a too small value of Δ, forces the system to have a poor or unstable performance. A rule of thumb is to define a value for Δ larger than twice the length of the robot (see e.g. [1]).

Motivated by the effective application of LOS guidance laws for path following control of marine surface vessels [1], [52] and especially in the corresponding case of ground snake robots [3], we choose the joint angle offset ϕ_0 as

$$\phi_0 = k_\theta \left(\bar{\theta} - \bar{\theta}_{\text{ref}}\right), \tag{19}$$

where $k_\theta > 0$ is a control gain [37].

C. Inner-Loop Controller

In order to make the joint angle ϕ_i follow its reference signal ϕ_i^*, a PD controller is used:

$$u_i = \ddot{\phi}_i^* + k_d(\dot{\phi}_i^* - \dot{\phi}_i) + k_p(\phi_i^* - \phi_i), \quad i = 1, \ldots, n-1, \tag{20}$$

where $k_p > 0$ and $k_d > 0$ are the gains of the controller.

Note that for the experimental and the simulation results presented in the following sections the values of the gait parameters α, ω, δ in (17) and the controller gains, k_p, k_d in (20) are chosen arbitrarily based on our experience on undulatory motion of underwater snake robots. In future, optimization techniques may be used for choosing the optimal gait parameters and preferably the controller gains should be based on model based analysis.

IV. Experimental Setup

This section describes the experimental setup employed for the fluid parameter identification and the investigation of the performance of the LOS path following controller proposed in [41].

A. Underwater Snake Robot – Mamba

In this section, the underwater snake robot that was used in our experiments is presented. A more detailed description of the robot can be found in [17].

Mamba (Fig. 5) is a snake robot that supports our group's research activity on both ground and underwater snake robot locomotion. This flexibility results from its mechanical robustness and reconfigurable nature. The robot is watertight and has a modular design with a common mechanical and electrical interface between the modules. Each joint module is actuated by a Hitec servo motor (HSR 5990TG) and in each joint, a force/torque sensor on the joint shaft, two temperature sensors, a 3-axis accelerometer and a water leakage detector, are included (Fig. 5). Furthermore, each joint is controlled by means of a microcontroller card (TITechSH2 Tiny Controller from HiBot), while the total number of microcontrollers intercommunicate over a CAN bus. Power supply cables (35 V) run among the modules along with the CAN bus. A more detailed description of this robot is found in [17].

Note that all the modules of the underwater snake robot Mamba are watertight down to about 5 m. However, during the experiments, Mamba was covered by a watertight skin in order to achieve an extra water barrier (Fig. 6). The skin is made by Groundsheet, Nylon, PU-coated, 120 g/m^2 material and it is attached at the head and the tail parts using rubber bottle wrist seals, which are glued to the skin. This type of cover makes the robot's outer surface smoother, reducing, in this way, the drag effects. In addition, it is worth mentioning that no caudal fin is attached at the tail part of the robot during the experiments since the model presented in Section II does not consider modeling of a caudal fin. Hence, the tail part only contains an anchorage mechanism for the external power supply cable.

B. Experimental setup

The experiments were performed in the MC-lab in Marintek, Trondheim, Norway [53], in a tank of dimensions L: 40 m, H: 1.5 m and W: 6.45 m. In order to have accurate real time measurements of the position and orientation of underwater objects, in general, the integration of a motion capturing system is essential. Thus, for our experimental process, an underwater motion capture system from Qualisys [54] was installed in the basin, covering an underwater working area of dimensions 10m$\times$1.35m$\times$ 5.45m.

The particular configuration of the snake robot Mamba [17], see Fig. 6, used in these experiments, consisted of 18 identical joint modules mounted horizontally and vertically in an alternating fashion (Fig. 5). By setting the reference angles for the joints with vertical rotating axis to be zero degrees, the robot was made to move according to a strictly horizontal motion pattern. In this case, the kinematics of the snake robot corresponds to a planar snake robot with links of length $2l = 0.18$ m and mass $m \approx 0.8$ kg. The experiments demonstrated that the robot had a slightly positive buoyancy and was swimming near the water surface.

In order to have accurate measurements of the robot's position and orientation, reflective markers were attached on the tail part of the robot, something that is required by the motion capturing system, as shown in Fig. 6. Although the robot was swimming on the surface of the tank, the markers were submerged, approximately 0.15 m under the water surface,

due to constraints in the covering working area imposed by the camera system. Thus, the global frame coordinates of the tail link and the absolute angle of the tail were extracted by the camera-based motion capture system. Especially, the camera system consists of six identical cameras, which allow reflective markers to be tracked under the water. The measured position and the absolute angle of the tail were obtained from an external computer where the Qualisys system [54] was connected, and afterwards these measurements were sent through UDP in LabVIEW 2013 to another computer where both the fluid parameters identification algorithms and the path following controller were implemented. Having the measurements of the tail position and orientation, and the individual joint angles, the center of mass position, $\mathbf{p}_{\text{CM}}$, and the absolute link angles, $\boldsymbol{\theta}$, of the underwater snake robot were calculated from the kinematics equations presented in Section II.

Remark 4. As previously mentioned, reflective markers were attached on the tail part of the robot in order to obtain the required measurements for the experiments. It is expected that the performance of the robot will be influenced by the external structure that is used to attach the reflective markers during the motion of the robot. Note that it is essential for an underwater camera system to have a stiff structure which is able to avoid any misplacement of the markers during the motion of the robot in order to provide accurate measurements, while the structure needs to have reasonable dimensions in order to reduce the effects on the motion of the robot. In order to reduce the influence of an external component attached to the snake, we implemented a lightweight and stiff structure made from iron ropes in which the markers were attached. In addition, note that the camera system from Qualisys is only proper for experimental work in the lab, while for real life applications available commercial solutions such as Long-baseline (LBL) systems, Ultra-short-baseline (USBL) systems or Underwater Wireless Sensor Networks (UWSNs) can be used. In [55], a survey of techniques for underwater localization is presented.

V. Model Identification

In this section, we present results regarding the fluid parameters identification for the model of the underwater snake robot presented in Section II. We obtained the values of the fluid coefficients by using the method of [14]. Note that the fluid parameters are identified in order to validate experimentally the closed-loop form model of underwater snake robots proposed in [2], and in addition it will be used for back-to-back comparison of simulation and experimental results for the path following control strategy presented in Section III.

A. Fluid Parameters

In [2], it is shown that the fluid force parameters, for cylindrical links with major diameter $2a$ and minor diameter $2b$ and taking into account that the length of each link is $2l$, are given by

$$c_t = \frac{1}{2}\rho\pi C_f \frac{(b+a)}{2} 2l, \tag{21}$$

$$c_n = \frac{1}{2}\rho C_D 2a 2l, \tag{22}$$

$$\mu_n = \rho\pi C_A a^2 2l, \tag{23}$$

where C_f and C_D are the drag coefficients in x and y direction of motion, while C_A denotes the added mass coefficient [56] and ρ is the density of the fluid.

In addition, it is shown that the fluid torque parameters can be expressed as

$$\lambda_1 = \frac{1}{12}\rho\pi C_M (a^2 - b^2)^2 l^3, \tag{24}$$

$$\lambda_2 = \frac{1}{6}\rho\pi C_f (a+b) l^3, \tag{25}$$

$$\lambda_3 = \frac{1}{8}\rho\pi C_f (a+b) l^4 \tag{26}$$

where C_M is the added inertia coefficient.

B. Fluid Parameter Identification

The fluid coefficients that will be identified are C_f, C_D and C_A. Note that the added mass inertia coefficient is set to the theoretical value $C_M = 1$ in this study since this parameter does not significantly affect the overall motion of the system [2], [25].

Using the underwater snake robot Mamba (Fig. 6) with the reflective markers attached on the tail of the robot, we were able to measure the position and the orientation of the tail module by using the camera system described in Section IV. Combining these measurements with the measurements of the joint angles and using the kinematic equations presented in Section II, we are able to calculate the position of the center of mass of the robot. As mentioned earlier, the robot is commanded to move according to a horizontal motion pattern in a horizontal plane, by setting the reference angles corresponding to the vertical joint motion to zero. Hence, only the joints with horizontal rotating axis are made to rotate, and the number of links is $n = 9$. This is because we need only measurements in the 2D horizontal plane for the fluid coefficients identification of the 2D fluid model presented in Section II. We applied the sinusoidal motion pattern given by (17) with different parameters. In particular, in each trial, the reference joint angles were computed by (17) for $n = 9$ choosing $\mathrm{g}(i,n) = 1$ and $\mathrm{g}(i,n) = (n-i)/(n+1)$ in case of lateral undulation and eel-like motion, respectively. These references were sent to the robot via the CAN. In each trial we measured the position of the center of mass and the steady state values of the achieved velocity for approximately 30 sec of motion. Note that an existing proportional controller, implemented in the microcontroller of each joint module, is responsible for the control of the corresponding joint angle. Finally, the initial values of the link angles were set to zero in each experiment task, while the initial position of the robot is presented in each trial.

In order to perform a back-to-back comparison of experimental data and ideal simulation results, we simulated the model of the underwater snake robot presented in Section II with the fluid coefficients found by curve fitting between one set of simulated data with one set of data from the motion of the physical robot, to be $C_f = 0.3$, $C_D = 1.75$, $C_A = 1.5$ for lateral undulation and $C_f = 0.17$, $C_D = 1.75$, $C_A = 1.5$ for eel-like motion. Note that the fluid coefficient C_f is smaller for the eel-like motion compared to the lateral undulation. This was expected since we have oscillations with smaller amplitude at the head of the robot, causing the effect of the drag forces in the x direction to be smaller. In particular, we

Fig. 5. The underwater snake robot Mamba implemented at NTNU to support our group's research activity about both ground and underwater snake robot locomotion.

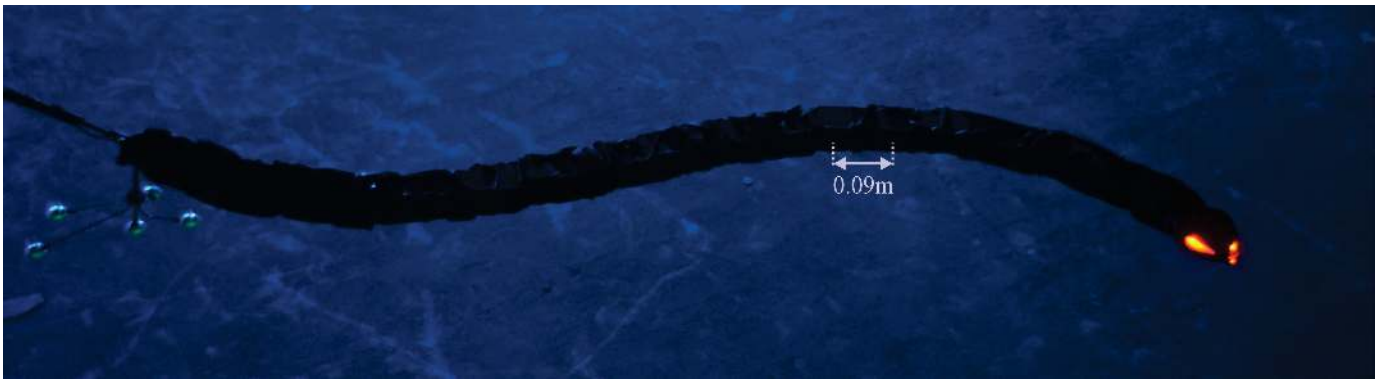

Fig. 6. The underwater snake robot Mamba in the pool with the markers attached on the tail for position measurements.

considered an underwater snake robot with $n = 9$ links, each one having length $2l = 0.18$ m and mass $m = 0.8$ kg, i.e. identical to the physical robot presented in Section IV.A. The hydrodynamic related parameters for the elliptic section with major and minor diameters $2a = 2 \cdot 0.055$ m and $2b = 2 \cdot 0.05$ m, respectively, and $\rho = 1000$ kg/m^3 were calculated by (21)-(26). In these simulations a joint PD-controller (20) was used with parameters $k_p = 20, k_d = 5$, while lateral undulation or eel-like motion were achieved by moving the joints according to (17) by choosing $\mathrm{g}(i, n) = 1$ and $\mathrm{g}(i, n) = (n-i)/(n+1)$, respectively, with gait parameters values similar to the ones of the experimental trials.

In Fig. 7 and 8, we present simulation and experimental results that were obtained by choosing the fluid coefficients as mentioned earlier and $\alpha = 30^o$, $\omega = 120^o/\mathrm{s}$, $\delta = 30^o$ and $\phi_0 = 0$ for lateral undulation and eel-like motion. The simulated and the experimental results are expressed in the global frame with the origin being at (0,0) for visualization purposes. This makes the comparison of the simulated and the experimental results clearer, without changing the response of the system. From Fig. 7a and Fig. 8a, we see that the robot managed to transverse the same distance in the x-direction both in simulations and in experiments. We see that the oscillations in the y-direction (Fig. 7b - Fig. 8b) are larger in the experimental trial compared to the simulated results. This is mostly due to the inaccuracies of the sensor measurements in the experimental setup. The achieved forward steady state velocity was calculated for the simulated and the physical robot by using

$$V_f^s = \sqrt{\dot{p_x}(t_{\text{end}})^2 + \dot{p_y}(t_{\text{end}})^2} \tag{27}$$

and

$$V_f^r = \frac{\sqrt{(p_x(t_{\text{end}}) - p_x(t_0))^2 + (p_y(t_{\text{end}}) - p_y(t_0))^2}}{t_{\text{end}} - t_0}, \tag{28}$$

respectively. Note that t_{end} and t_0 indicate the beginning and the end of the time horizon, respectively. The amplitudes of the achieved forward steady state velocities for the lateral undulation calculated by (27) and (28), were 0.1275 m/s and 0.1288 m/s for the simulated robot and the real robot, respectively. The error between these velocities was 1.01 %, which indicates that there is quite good agreement between the simulated dynamics of the robot and the real experiments. In addition, the steady state velocities for the eel-like motion were 0.0897 m/s and 0.0894 m/s for the simulated robot and

TABLE II
FLUID PARAMETER IDENTIFICATION FOR LATERAL UNDULATION

α	ω	δ	V_f^s	V_f^r	Error %
30	120	20	0.1207	0.1275	5.37
30	120	30	0.1275	0.1288	1.01
30	120	50	0.0851	0.0937	9.11
30	110	30	0.1153	0.1281	10.03
30	130	30	0.1252	0.1179	6.21

TABLE III
FLUID PARAMETER IDENTIFICATION FOR EEL-LIKE MOTION

α	ω	δ	V_f^s	V_f^r	Error %
30	120	20	0.0742	0.0756	1.88
30	120	30	0.0897	0.0894	0.33
30	120	50	0.0723	0.0738	1.98
30	110	30	0.0867	0.0996	12.92
30	130	30	0.0927	0.0885	4.81

the real robot, respectively. The error between the velocities for the case of eel-like motion was 0.33 %.

In addition, by keeping the chosen values for the fluid coefficients constant, we obtained comparable results between the simulation and experimental results both for the lateral undulation and eel-like motion pattern. In Table II and III, we can see the achieved forward velocities both for the simulated and the physical system for different values of the gait parameters. In particular, the first three columns of the tables present the values of the gait parameters, while the last three columns present the forward velocity of the simulated robot, the velocity of the physical robot and the relative error between the forward velocities, respectively. From Table II and III, we can see that the maximum error between the simulated and the physical robot was 10.03% and 12.92% for the lateral undulation and eel-like motion pattern, respectively. These preliminary results show that the fluid coefficients are quite sensitive to variations of the gait parameters. However, in [14] it was also shown that for the swimming speed the discrepancies between modeling and reality do not exceed 16%.

Remark 5. Note that another more accurate method for the fluid coefficients identification should be investigated in the future for more precise identified values of the drag and added mass coefficients since, as we can see from Table II and III, the identified fluid coefficients are quite sensitive to variations of the gait parameters. In this study, preliminary results are obtained for the model presented in Section II, which mainly will be used to investigate the efficacy of the path following controller presented in Section III by comparing the experimental results with the simulated ones. In the future, the force/torque sensor installed inside the modules of the snake robot may be used in order to obtain more general results for the fluid coefficients, avoiding the calculation of these coefficients by fitting the simulated motion with the motion of the physical robot.

VI. EXPERIMENTAL INVESTIGATION OF LOS PATH FOLLOWING CONTROLLER

In this section, the experimental results will be presented in order to investigate the efficacy of the LOS path following controller presented in Section III. In particular the performance of the guidance strategy was investigated experimentally for straight line paths for both lateral undulation and eel-like motion patterns.

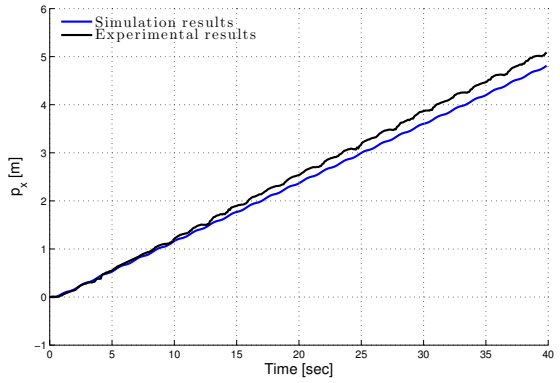

(a) Position along the path, p_x

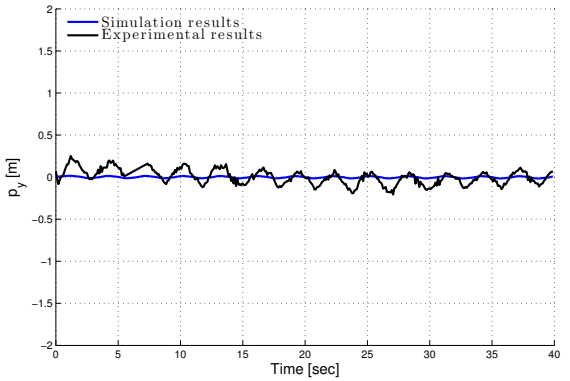

(b) Position along the path, p_y

Fig. 7. Lateral undulation: Comparison results of the simulated and real robot for the gait parameters $\alpha = 30^o$, $\omega = 120^o/\text{s}$, $\delta = 30^o$ and $\phi_0 = 0$.

A. Experimental setup

The path following controller was experimentally investigated using the underwater snake robot Mamba (see Fig. 5). The total control structure that was adopted in the experimental task is illustrated in Fig. 9. The individual computations and the implementation of the path following controller are described in the sequel steps. Having the measurements of the tail position and orientation, and the individual joint angles, we calculated, using the kinematics equations presented in Section II, the center of mass position, $\mathbf{p}_{\text{CM}}$, and the absolute link angles, $\boldsymbol{\theta}$, of the underwater snake robot. The LOS path following controller of the underwater snake robot was implemented on an external computer according to (17), (18) and (19), i.e. the for the lateral undulation and eel-like motion gait patterns. Specifically, the reference joint angles, computed by (17), were sent to each joint module of the robot via the CAN bus running through the robot. A proportional controller implemented in the microcontroller of each joint module controlled the joint angle according to the received reference angle. The joint torque controller given by (20) was not implemented, since the servo motors installed in the snake robot do not require torque control input as the servos have built in angle regulation. The robot's orientation was calculated

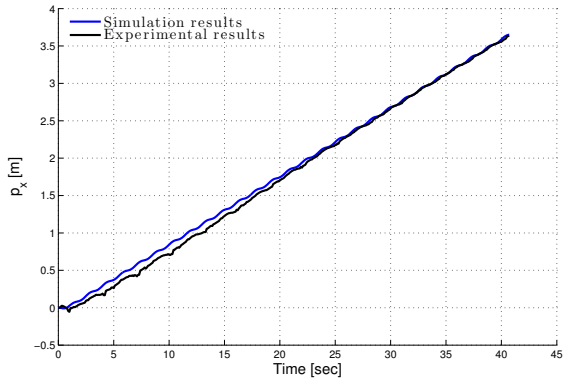

(a) Position along the path, p_x

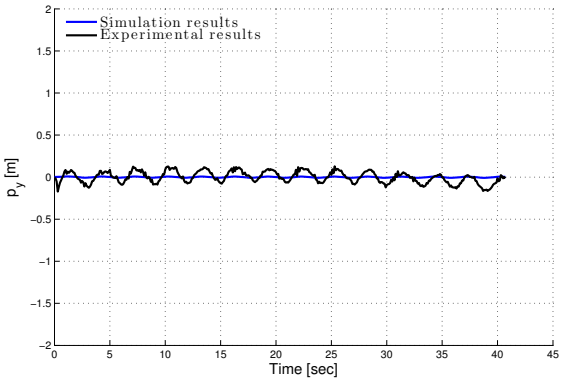

(b) Position along the path, p_y

Fig. 8. Eel-like motion: Comparison results of the simulated and real robot for the gait parameters $\alpha = 30^o$, $\omega = 120^o/\text{s}$, $\delta = 30^o$ and $\phi_0 = 0$.

according to (2), i.e. as the average of the individual link angles.

The LOS guidance law angle given by (18) was calculated with a look-ahead distance equal to half the length of the robot, i.e. $\Delta = 0.9$ m [1] for fast convergence, due to the limited working area covered by the camera system. Furthermore, the control gain in (19) was $k_\theta = 0.4$ and $k_\theta = 0.6$ for lateral undulation and eel-like motion, respectively. The joint angle offset was saturated according to $\phi_0 = [-20^o, 20^o]$ in order to keep the joint reference angles within reasonable bounds and taking into account the physical robot's joint angle constraints. Moreover, the reference angles were calculated by (17) for $n = 9$ choosing $\text{g}(i, n) = 1$ and $\text{g}(i, n) = (n - i)/(n + 1)$ in case of lateral undulation or eel-like motion, respectively, while the rest of the gait parameters were $\alpha = 35^\text{o}$ for lateral undulation and $\alpha = 40^\text{o}$ for eel-like motion, $\delta = 40^\text{o}$ and $\omega = 120^\text{o}/\text{s}$. The initial joint angles were zero in all the trials, while the initial heading and position of the robot will be specified for each trial.

B. Experimental Results

The straight line path following controller was experimentally investigated for both lateral undulation and eel-like motion patterns. In particular, experimental results for two different sets of initial conditions are presented here, both for lateral undulation and eel-like motion patterns. In the first four trials of the experiments, the robot was initially headed along the desired path (the x axis), and the initial distance from the CM to the desired path was 1.89 m and 2.81 m for lateral undulation (Fig. 10-11) and 2.75 m and 2.98 m for eel-like motion (Fig. 12-13). In the last two trials, the robot was initially headed towards the desired path (the x axis) with initial heading $\bar{\theta}(0) = -91.3^o$ and $\bar{\theta}(0) = -88.3^o$, for lateral undulation (Fig. 14) and eel-like motion (Fig. 15), and the initial distance from the CM to the desired path was 1.59 m and 1.97 m, respectively. The xy-plots of the experimental results for the different trials are presented in Fig. 10a, Fig. 11a, Fig. 14a for lateral undulation and Fig. 12a, Fig.13a, Fig. 15a for eel-like motion pattern, where it is easily seen that the robot converged nicely towards and moved along the desired path during all trials both for lateral undulation and eel-like motion patterns. In particular, we can see that the center of mass of the underwater snake robot converged to the desired path for all the trials.

In Fig. 10d - 15d we can see that (19) made the heading angle converge to and oscillate around zero for both lateral undulation and eel-like motion patterns. Moreover, Fig. 10c-15c show that the cross track error converged to and oscillated around zero. Furthermore, the forward velocity of the robot is shown in Fig. 10e - 15e and the joint angle offset is shown in Fig. 10f - 15f. Fig. 10-15 clearly show that the heading, the cross track error and the position of the robot achieved a steady state oscillatory behavior when the robot reached the desired path. Note that this was as expected since for snake robots forward locomotion is achieved using a sinusoidal gait pattern, and it is then not possible to achieve a purely non-oscillating motion of the CM [57]. Similar to the oscillatory behaviour of the CM, the orientation of the robot was also expected to oscillate, as it is shown in Fig. 10d - 15d.

The visualisations in Fig. 16 and Fig. 17 for the results presented in Fig. 10 and Fig. 12 for lateral undulation and eel-like motion, respectively, illustrate that the robot converged nicely towards and moved along the desired path. This claim is supported by the plots of the cross-track error in Fig. 10c and Fig. 12c, which shows that the cross-track error converged to and oscillated about zero.

C. Simulation Results

In order to perform a back-to-back comparison of real experimental and ideal simulation results, we simulated the model presented in Section II with the LOS path following controller proposed in Section III using similar parameters as in the experiments. In particular, we considered an underwater snake robot with $n = 9$ links, each one having length $2l = 0.18$ m and mass $m = 0.8$ kg, i.e. identical to the physical robot presented in Section VI.A. The hydrodynamic parameters c_t, c_n, μ_n λ_1, λ_2 and λ_3 were calculated for the fluid coefficients C_f, C_d and C_A as identified in Section V. The joint PD controller (20) was used for each joint with parameters $k_p = 20$, $k_d = 5$, and the reference angles corresponding to the horizontal joint motion of the robot were calculated according to (17) with $n = 9$ by choosing $\text{g}(i, n) = 1$ and $\text{g}(i, n) = (n-i)/(n+1)$ for lateral undulation and eel-like motion respectively, with the same gait parameters as presented in Section V.B. Furthermore, the control gain in (19) is $k_\theta = 0.4$ and $k_\theta = 0.6$ for lateral undulation and eel-like motion, respectively, while the guidance law parameter in (18) was chosen as $\Delta = 0.9$ similar to the experimental trials. The initial values of all states of the robot

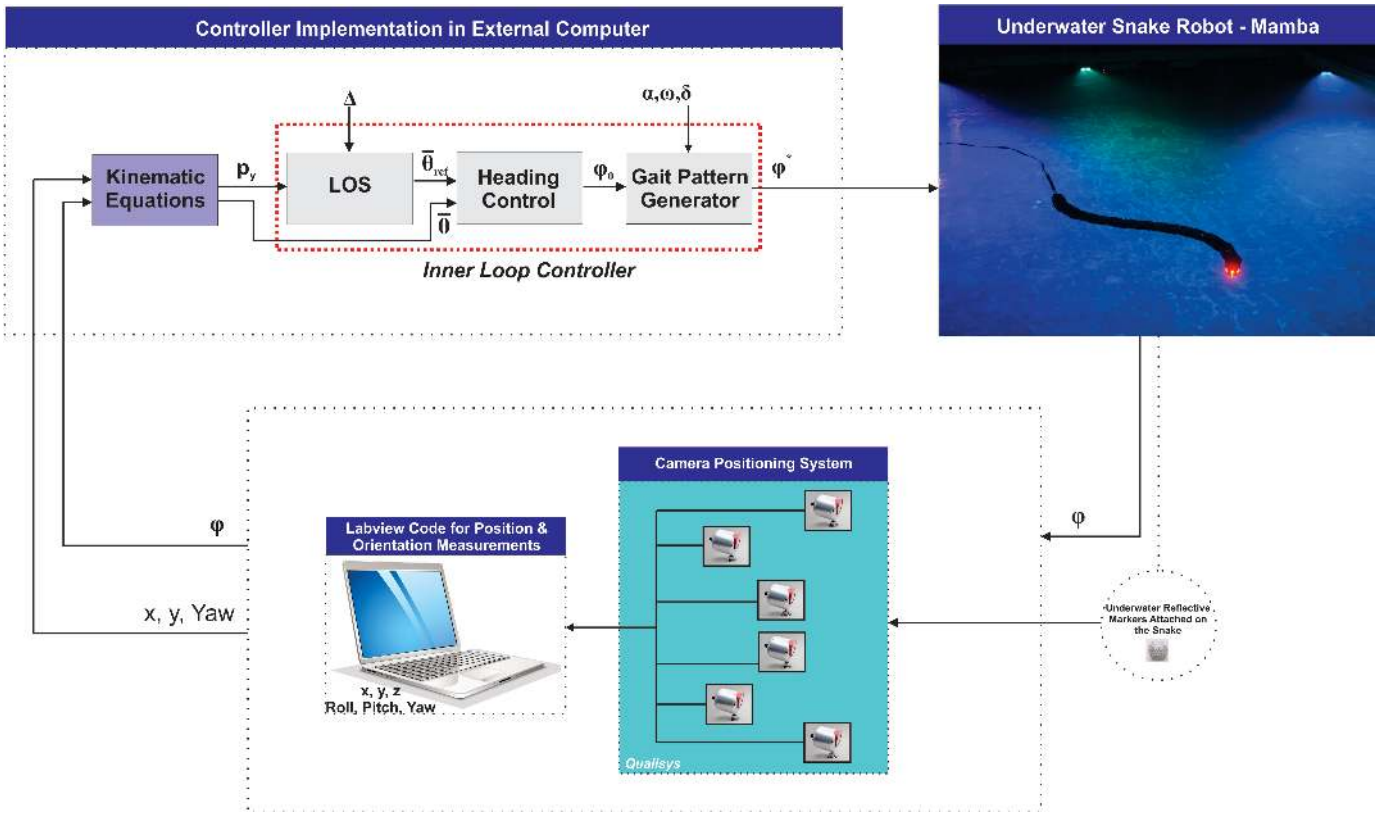

Fig. 9. Illustration of the controller structure used in the experiments, with the markers attached to the tail of the robot for position measurements.

were set to zero except for the initial position of the center of mass, which was selected as $p_{CM}(0) = [-3.58, 1.89]$ and $p_{CM}(0) = [-4.20, 2.75]$ for lateral undulation and eel-like motion, respectively, i.e. the same as the initial values of the experiments presented in Fig. 10 and Fig. 12. The simulation results are shown in Fig. 18 and Fig. 19. In addition, Fig. 20 and Fig. 21 present comparison results for the cross track error and the heading between the simulated and the physical robot.

The results shown in Fig. 18, Fig. 19, Fig. 20 and Fig. 21 indicate that the qualitative behavior of the simulated system is similar to the behavior of the physical robot. In particular, from Fig. 10a, Fig. 12a and Fig. 18a, Fig. 19a it can be seen that the physical snake and the simulated snake followed almost the same path for both lateral undulation and eel-like motion patterns. The cross track error converged and oscillated around zero for both motion patterns, as shown in Fig. 10c, Fig. 12c, Fig. 20b and Fig. 18c, Fig. 19c, Fig. 21b. Fig. 10c, Fig. 12c show that the cross-track error had larger oscillations compared to the ideal case in Fig. 18c, Fig. 19c. This was expected mainly due to the noise on the measurements in the experiments caused by the different sensors, i.e. noise on the position measurement from the camera system and the joint angle measurements from the actuators. From Fig. 10d, Fig. 12d, Fig. 20a and Fig. 18d, Fig. 19d, Fig. 21a we see that in both cases the heading converged zero. The oscillations of the heading are larger in Fig. 10d, Fig. 12d than in Fig. 18d, Fig. 19d and this is again due to the inaccuracies of the different measurements from the sensors. Note that the heading is defined as the average of the link angles (2) and any inaccurate measurements from the encoders will produce errors, and this is the main reason for the larger oscillations in the heading in the experimental results presented in Fig. 10d, Fig. 12d.

Remark 6. It should be noted that in [34], [41] in order to investigate the performance of the path following control strategies, the fluid coefficients were chosen under the the assumption of a steady-state flow [36], [58]. In this paper, however, simulation results for the LOS path following controller are performed for the the drag and added mass coefficients of the system identified experimentally in Section V.

Remark 7. Comparing the experimental results (Fig. 10, Fig. 12) with the simulated ones (Fig. 18, Fig. 19), we see that the simulated model reached higher velocities both for lateral undulation and eel-like motion. This was mainly due to the power supply cable that was attached to the robot. Note that in our simulations we did not have the extra drag effects that were produced from the power supply cable of the physical robot that was used in the experiments. The effect of this cable is more visible for the slower motion achieved for the eel-like motion pattern (Fig. 12 and Fig. 19). However, comparison results presented in Fig. 20 and Fig. 21 show good agreement between the simulated and the physical robot for the cross-track error and the heading both for lateral undulation and eel-like motion patterns.

VII. Conclusions and Future Work

In this work experimental results for line-of-sight path following control of biologically inspired swimming snake robots were presented. In particular, a straight line path following controller was proposed for an underwater snake robot, both for lateral undulation and eel-like motion patterns. The LOS guidance law was combined with a directional controller to

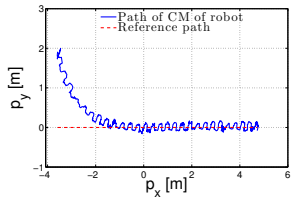

(a) Path of the CM

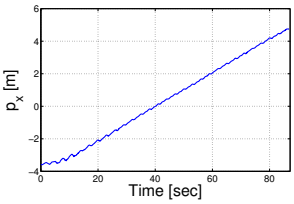

(b) Position along the path, p_x

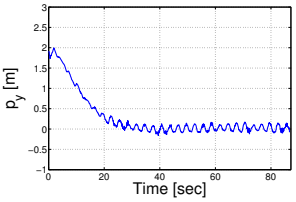

(c) Cross-track error, p_y

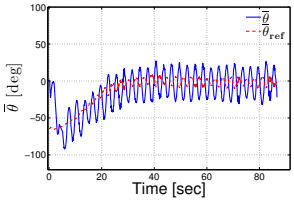

(d) Heading angle, $\overline{\theta}$

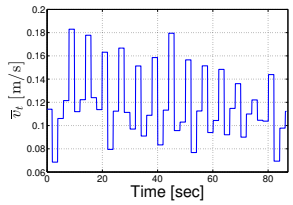

(e) Forward Velocity, $\overline{v}_t$

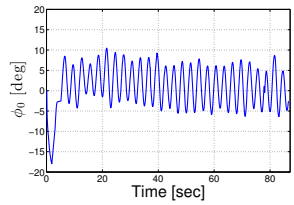

(f) Joint angle offset, ϕ_0

Fig. 10. Straight line path following with the physical snake initially headed along the desired path, and with the initial distance from the CM being $p_y = 1.89$ m for lateral undulation with gait parameters $\alpha = 35^o$, $\omega = 120^o/\text{s}$ and $\delta = 40^o$.

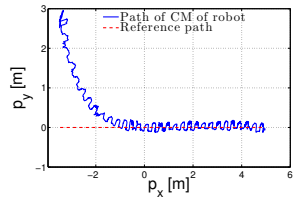

(a) Path of the CM

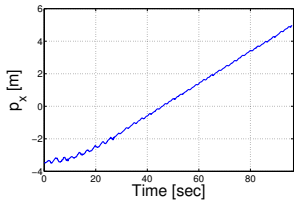

(b) Position along the path, p_x

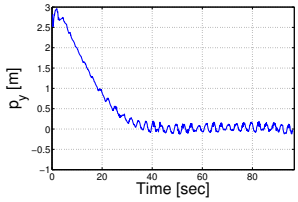

(c) Cross-track error, p_y

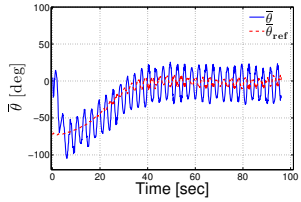

(d) Heading angle, $\overline{\theta}$

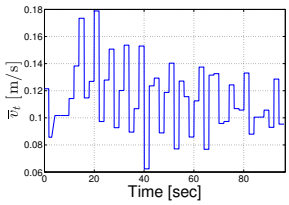

(e) Forward Velocity, $\overline{v}_t$

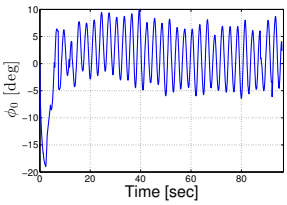

(f) Joint angle offset, ϕ_0

Fig. 11. Straight line path following with the physical snake initially headed along the desired path, and with the initial distance from the CM being $p_y = 2.81$ m for lateral undulation with gait parameters $\alpha = 35^o$, $\omega = 120^o/\text{s}$ and $\delta = 40^o$.

steer the robot to the path. The proposed path following controller consists of three main components: a) the gait pattern controller, which produces a sinusoidal motion pattern which propels the robot forward, b) the heading controller, which steers the robot towards and subsequently along the desired path and c) the LOS guidance law, which generates the desired heading angle in order to follow the desired path. It was shown that the proposed control scheme can be applied to underwater snake robots to achieve path following of straight lines. In addition, fluid parameter identification was performed and simulation results based on the identified fluid coefficients were presented to obtain a back-to-back comparison with the motion of the physical robot during the experiments. The experimental results showed that the proposed control strategy successfully steers the robot towards and along the desired path for both lateral undulation and eel-like motion patterns.

In future work, the authors will investigate the validity of the proposed control strategy for general path following control purposes. In this paper, we did not take into account the current effects since there is no possibility to produce current at the MC-laboratory. It is furthermore of interest to test the scheme for the fluid coefficient identification in combination with current effects in the future. The force/torque sensors installed inside the modules of the robot may be used for more precise online fluid coefficient identification with and without the current effects. In addition, an interesting topic for future work concerns the possibility to extend the proposed control approach to 3D and thus be able to investigate depth control strategies for underwater snake robots. An experimental investigation of path following of underwater snake robots in 3D is necessary in order to realize underwater snake robots for challenging real time subsea operations.

REFERENCES

[1] T. I. Fossen, *Handbook of Marine Craft Hydrodynamics and Motion Control*. John Wiley & Sons, Ltd, 2011.

[2] E. Kelasidi, K. Y. Pettersen, J. T. Gravdahl, and P. Liljebäck, "Modeling of underwater snake robots," in *Proc. IEEE International Conference on Robotics and Automation (ICRA)*, Hong Kong, China, May 31-June 7 2014, pp. 4540–4547.

[3] P. Liljebäck, K. Y. Pettersen, Ø. Stavdahl, and J. T. Gravdahl, *Snake Robots: Modelling, Mechatronics, and Control*. Springer-Verlag, Advances in Industrial Control, 2013.

[4] ——, "A review on modelling, implementation, and control of snake robots," *Robotics and Autonomous Systems*, vol. 60, no. 1, pp. 29–40, 2012.

[5] A. A. Transeth and K. Y. Pettersen, "Developments in snake robot modeling and locomotion," in *Proc. 9th International Conference on Control, Automation, Robotics and Vision (ICARCV)*, Singapore, Dec. 5-8 2006, pp. 1–8.

[6] J. Gray, "Studies in animal locomotion," *The Journal of Experimental Biology*, vol. 10, no. 1, pp. 88–104, 1933.

[7] S. Hirose, *Biologically Inspired Robots: Snake-Like Locomotors and Manipulators*. Oxford University Press, 1993.

[8] S. Hirose and H. Yamada, "Snake-like robots [tutorial]," *IEEE Robotics Automation Magazine*, vol. 16, no. 1, pp. 88–98, 2009.

[9] R. Crespi, A. Badertscher, A. Guignard, and A. J. Ijspeert, "Amphibot I: an amphibious snake-like robot," *Robotics and Autonomous Systems*, vol. 50, no. 4, pp. 163–175, 2005.

[10] P. Liljebäck, K. Y. Pettersen, and Ø. Stavdahl, "A snake robot with a contact force measurement system for obstacle-aided locomotion," in *Proc. IEEE International Conference on Robotics and Automation (ICRA)*, Anchorage, AK, USA, May 3-7 2010, pp. 683–690.

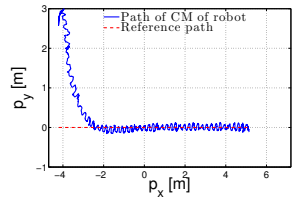

(a) Path of the CM

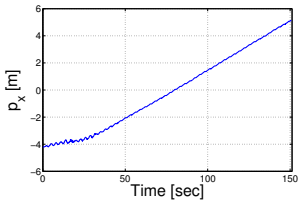

(b) Position along the path, p_x

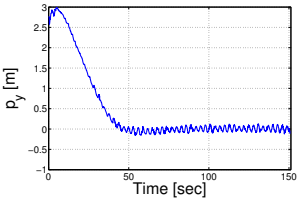

(c) Cross-track error, p_y

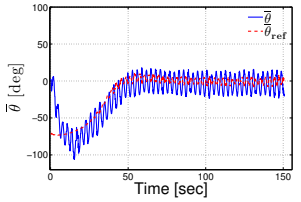

(d) Heading angle, $\overline{\theta}$

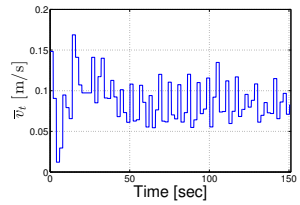

(e) Forward Velocity, $\overline{v}_t$

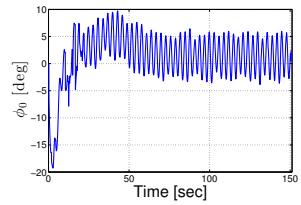

(f) Joint angle offset, ϕ_0

Fig. 12. Straight line path following with the physical snake initially headed along the desired path, and with the initial distance from the CM being $p_y = 2.75$ m for eel-like motion with gait parameters $\alpha = 40^o$, $\omega = 120^o/\text{s}$ and $\delta = 40^o$.

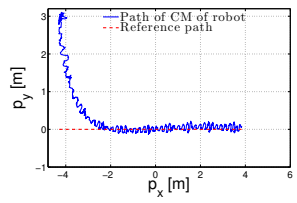

(a) Path of the CM

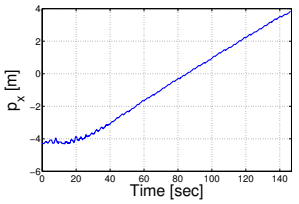

(b) Position along the path, p_x

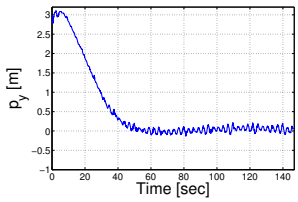

(c) Cross-track error, p_y

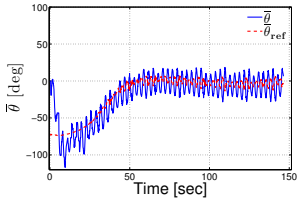

(d) Heading angle, $\overline{\theta}$

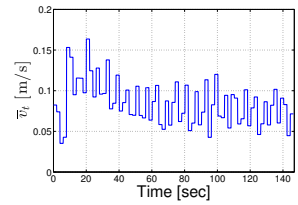

(e) Forward Velocity, $\overline{v}_t$

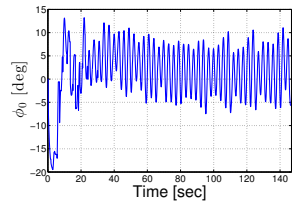

(f) Joint angle offset, ϕ_0

Fig. 13. Straight line path following with the physical snake initially headed along the desired path, and with the initial distance from the CM being $p_y = 2.98$ m for eel-like motion with gait parameters $\alpha = 40^o$, $\omega = 120^o/\text{s}$ and $\delta = 40^o$.

[11] K. Melsaac and J. Ostrowski, "A geometric approach to anguilliform locomotion: modelling of an underwater eel robot," in *Proc. International Conference on Robotics and Automation (ICRA)*, vol. 4, Detroit, MI, May 10-15 1999, pp. 2843–2848.

[12] K. McIsaac and J. Ostrowski, "Experiments in closed-loop control for an underwater eel-like robot," in *Proc. IEEE International Conference on Robotics and Automation (ICRA)*, Washington DC, May 12-18 2002, pp. 750–755.

[13] A. Crespi and A. J. Ijspeert, "AmphiBot II: An Amphibious Snake Robot that Crawls and Swims using a Central Pattern Generator," in *Proc. 9th International Conference on Climbing and Walking Robots (CLAWAR)*, Brussels, Belgium, Sept. 2006, pp. 19–27.

[14] M. Porez, F. Boyer, and A. J. Ijspeert, "Improved lighthill fish swimming model for bio-inspired robots: Modeling, computational aspects and experimental comparisons," *The International Journal of Robotics Research*, vol. 33, no. 10, pp. 1322–1341, 2014.

[15] C. Ye, S. Ma, B. Li, and Y. Wang, "Locomotion control of a novel snake-like robot," in *Proc. IEEE/RSJ International Conference on Intelligent Robots and Systems (IROS)*, Sendai, Japan, Sept. 28-02 2004, pp. 925–930 vol.1.

[16] H. Yamada, S. Chigisaki, M. Mori, K. Takita, K. Ogami, and S. Hirose, "Development of amphibious snake-like robot ACM-R5," in *Proc. 36th International Symposium on Robotics*, Tokyo, Japan, 2005.

[17] P. Liljebäck, Ø. Stavdahl, K. Pettersen, and J. Gravdahl, "Mamba - a waterproof snake robot with tactile sensing," in *Proc. International Conference on Intelligent Robots and Systems (IROS)*, Chicago, IL, Sept. 14-18 2014, pp. 294–301.

[18] K. Morgansen, B. Triplett, and D. Klein, "Geometric methods for modeling and control of free-swimming fin-actuated underwater vehicles," *IEEE Transactions on Robotics*, vol. 23, no. 6, pp. 1184–1199, 2007.

[19] M. Kruusmaa, P. Fiorini, W. Megill, M. De Vittorio, O. Akanyeti, F. Visentin, L. Chambers, H. El Daou, M.-C. Fiazza, J. Jezov, M. Listak, L. Rossi, T. Salumae, G. Toming, R. Venturelli, D. Jung, J. Brown, F. Rizzi, A. Qualtieri, J. Maud, and A. Liszewski, "Filose for svenning: A flow sensing bioinspired robot," *IEEE Robotics Automation Magazine*, vol. 21, no. 3, pp. 51–62, 2014.

[20] G. Taylor, "Analysis of the swimming of long and narrow animals," *Proc. Royal Society of London. Series A. Mathematical and Physical Sciences*, vol. 214, no. 1117, pp. 158–183, 1952.

[21] M. J. Lighthill, "Large-amplitude elongated-body theory of fish locomotion," *Proc. Royal Society of London. Series B. Biological Sciences*, vol. 179, no. 1055, pp. 125–138, 1971.

[22] K. McIsaac and J. Ostrowski, "Motion planning for anguilliform locomotion," *IEEE Transactions on Robotics and Automation*, vol. 19, no. 4, pp. 637–625, 2003.

[23] F. Boyer, M. Porez, and W. Khalil, "Macro-continuous computed torque algorithm for a three-dimensional eel-like robot," *IEEE Transactions on Robotics*, vol. 22, no. 4, pp. 763 –775, 2006.

[24] J. Chen, W. O. Friesen, and T. Iwasaki, "Mechanisms underlying rhythmic locomotion: body-fluid interaction in undulatory swimming," *Journal of Experimental Biology*, vol. 214, no. 4, pp. 561–574, 2011.

[25] A. Wiens and M. Nahon, "Optimally efficient swimming in hyper-redundant mechanisms: control, design, and energy recovery," *Bioinspiration & Biomimetics*, vol. 7, no. 4, p. 046016, 2012.

[26] J. Blair and T. Iwasaki, "Optimal gaits for mechanical rectifier systems," *IEEE Transactions on Automatic Control*, vol. 56, no. 1, pp. 59–71, 2011.

[27] F. Candelier, M. Porez, and F. Boyer, "Note on the swimming of an elongated body in a non-uniform flow," *Journal of Fluid Mechanics*, vol. 716, pp. 616–637, 2013.

[28] L. Zhu, Z. Chen, and T. Iwasaki, "Oscillation, orientation, and locomotion of underactuated multilink mechanical systems," *IEEE Transactions on Control Systems Technology*, vol. 21, no. 5, pp. 1537–1548, 2013.

[29] J. Colgate and K. Lynch, "Mechanics and control of swimming: A review," *IEEE Journal of Oceanic Engineering*, vol. 29, no. 3, pp. 660–673, 2004.

[30] J. Liu and H. Hu, "Biological inspiration: from carangiform fish to multi-joint robotic fish," *Journal of Bionic Engineering*, vol. 7, pp. 35–48, 2010.

[31] R. Clapham and H. Huosheng, "iSplash-II: realizing fast carangiform swimming to outperform a real fish," in *Proc. IEEE/RSJ International Conference on Intelligent Robots and Systems (IROS)*, Chicago, Illinois, Sept. 14-18 2014, pp. 1080–1086.

[32] D. Jung, P. Pott, T. Salumae, and M. Kruusmaa, "Flow-aided path following of an underwater robot," in *Proc. IEEE International Conference on Robotics and Automation (ICRA)*, Karlsruhe, Germany, May 6-10 2013, pp. 4602–4607.

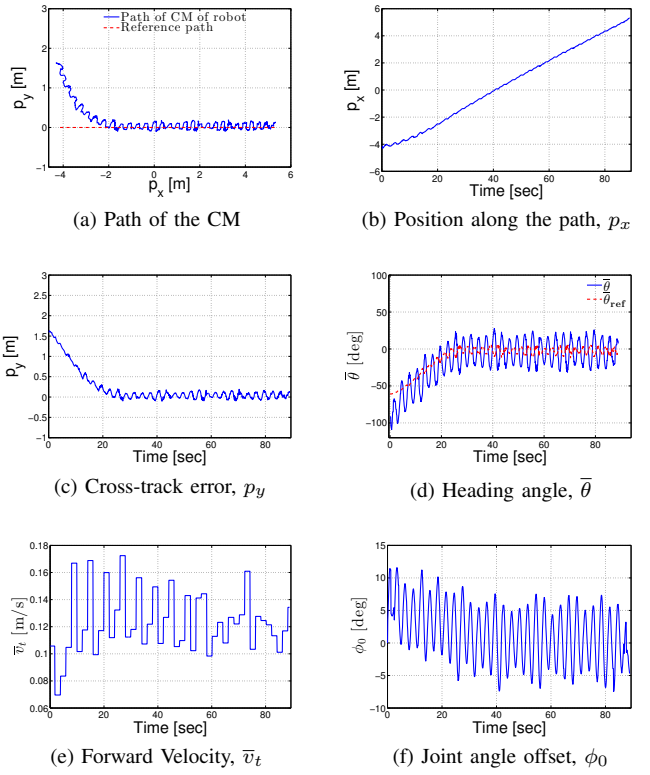

(a) Path of the CM (b) Position along the path, p_x

(c) Cross-track error, p_y (d) Heading angle, $\overline{\theta}$

(e) Forward Velocity, $\overline{v}_t$ (f) Joint angle offset, ϕ_0

Fig. 14. Straight line path following with the physical snake initially headed towards the desired path, and with the initial heading and the distance from the CM being $\bar{\theta}(0) = -91.3^o$ and $p_y = 1.59$ m, respectively, for lateral undulation with gait parameters $\alpha = 35^o$, $\omega = 120^o/\text{s}$ and $\delta = 40^o$.

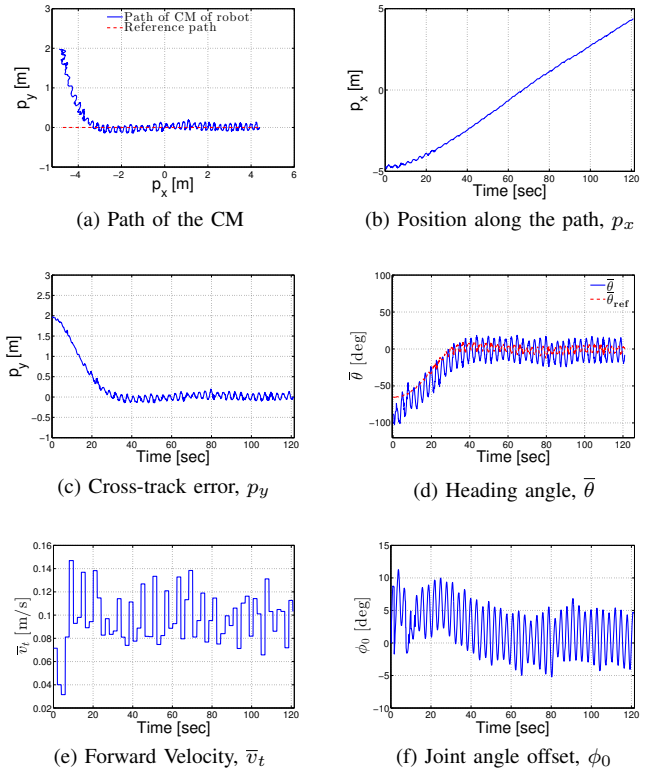

(a) Path of the CM (b) Position along the path, p_x

(c) Cross-track error, p_y (d) Heading angle, $\overline{\theta}$

(e) Forward Velocity, $\overline{v}_t$ (f) Joint angle offset, ϕ_0

Fig. 15. Straight line path following with the physical snake initially headed towards the desired path, and with the initial heading and the distance from the CM being $\bar{\theta}(0) = -88.3^o$ and $p_y = 1.97$ m, respectively, for eel-like motion with gait parameters $\alpha = 40^o$, $\omega = 120^o/\text{s}$ and $\delta = 40^o$.

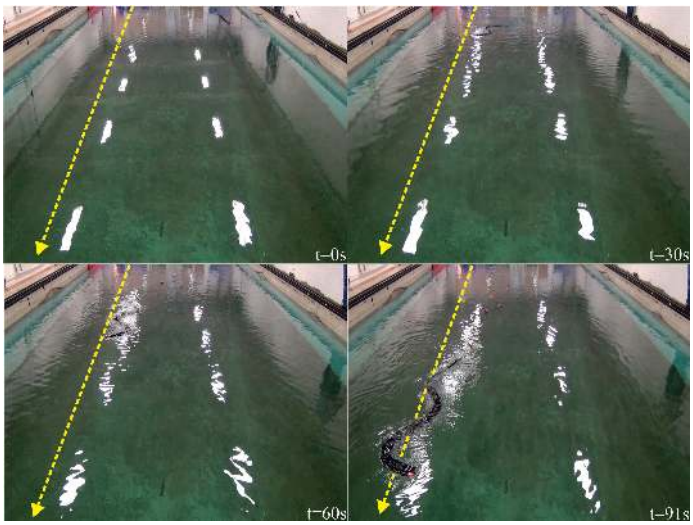

Fig. 16. The motion of the underwater snake robot during path following for the experimental results presented in Fig. 10. The *yellow line* indicates the desired path, i.e. the global x axis.

[33] Y. Ding, S. S. Sharpe, A. Masse, and D. I. Goldman, "Mechanics of undulatory swimming in a frictional fluid," *PLoS Computational Biology*, vol. 8, no. 12, p. e1002810, 2012.

[34] E. Kelasidi, P. Liljebäck, K. Y. Pettersen, and J. T. Gravdahl, "Integral line-of-sight guidance for path following control of underwater snake robots: Theory and experiments," in *IEEE Transactions on Robotics*, 2014, (Submitted).

[35] O. Ekeberg, "A combined neuronal and mechanical model of fish swimming," *Biological Cybernetics*, vol. 69, no. 5-6, pp. 363–374, 1993.

[36] W. Khalil, G. Gallot, and F. Boyer, "Dynamic modeling and simulation of a 3-D serial eel-like robot," *IEEE Transactions on Systems, Man, and Cybernetics, Part C: Applications and Reviews*, vol. 37, no. 6, pp. 1259–1268, 2007.

[37] E. Kelasidi, K. Y. Pettersen, P. Liljebäck, and J. T. Gravdahl, "Integral line-of-sight for path-following of underwater snake robots," in *Proc. IEEE Multi-Conference on Systems and Control*, Juan Les Antibes, France, Oct. 8-10 2014, pp. 1078 – 1085.

[38] K. McIsaac and J. Ostrowski, "Open-loop verification of motion planning for an underwater eel-like robot," in *Experimental Robotics VII*, ser. Lecture Notes in Control and Information Sciences, D. Rus and S. Singh, Eds. Springer Berlin - Heidelberg, 2001, vol. 271, pp. 271–280.

[39] P. A. Vela, K. A. Morgansen, and J. W. Burdick, "Underwater locomotion from oscillatory shape deformations," in *Proc. 41st IEEE Conference on Decision and Control (CDC)*, vol. 2, Las Vegas, USA, Dec. 10-13 2002, pp. 2074–2080.

[40] K. McIsaac and J. Ostrowski, "A framework for steering dynamic robotic locomotion systems," *International Journal of Robotics Research*, vol. 22, no. 2, pp. 83–97, 2003.

[41] E. Kelasidi, K. Y. Pettersen, and J. T. Gravdahl, "A waypoint guidance strategy for underwater snake robots," in *Proc. IEEE 22nd Mediterranean Conference on Control and Automation*, Palermo, Italy, June 16-19 2014, pp. 1512–1519.

[42] J. Guo, "A waypoint-tracking controller for a biomimetic autonomous underwater vehicle," *Ocean Engineering*, vol. 33, no. 17-18, pp. 2369 – 2380, 2006.

[43] M. Alamir, M. El Rafei, G. Hafidi, N. Marchand, M. Porez, and F. Boyer, "Feedback design for 3D movement of an eel-like robot," in *Proc. IEEE International Conference on Robotics and Automation (ICRA)*, Roma, Apr. 10-14 2007, pp. 256–261.

[44] M. El Rafei, M. Alamir, N. Marchand, M. Porez, and F. Boyer, "Motion control of a three-dimensional eel-like robot without pectoral fins," *Proc. 17th IFAC World Congress*, vol. 17, no. 1, pp. 750–755, 2008.

[45] ——, "Multi-variable constrained control approach for a three-dimensional eel-like robot," in *Proc. IEEE/RSJ International Conference on Intelligent Robots and Systems (IROS)*, Nice, France, Sept. 22-26 2008, pp. 3152–3157.

[46] L. Lapierre and B. Jouvencel, "Path following control for an eel-like

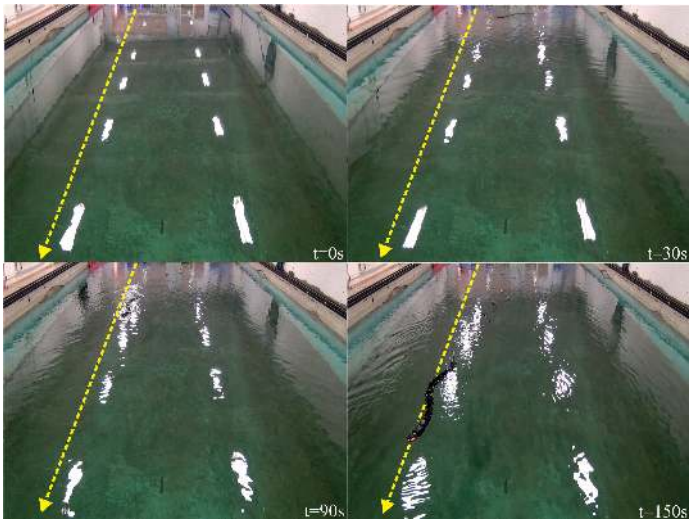

Fig. 17. The motion of the underwater snake robot during path following for the experimental results presented in Fig. 12. The *yellow line* indicates the desired path, i.e. the global x axis.

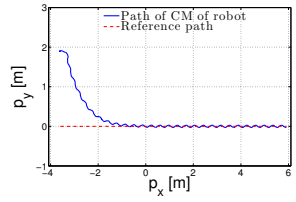

(a) Path of the CM

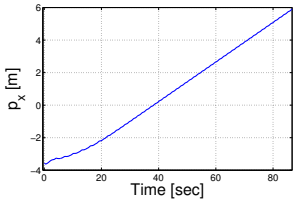

(b) Position along the path, p_x

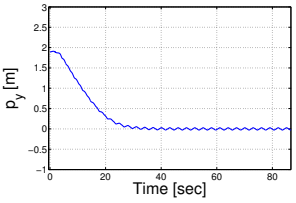

(c) Cross-track error, p_y

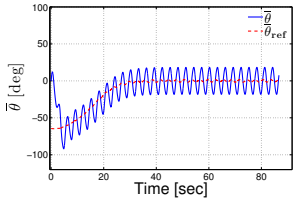

(d) Heading angle, $\overline{\theta}$

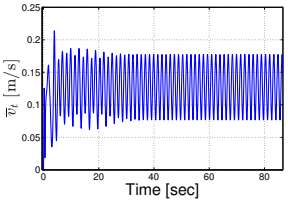

(e) Forward velocity, $\overline{v}_t$

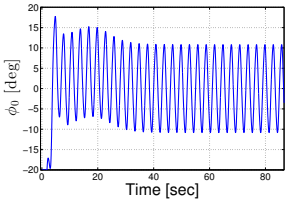

(f) Joint angle offset, ϕ_0

Fig. 18. Simulation results for straight line path following for a snake robot with $n = 9$ links initially headed along the desired path, and with the initial distance from the CM being $p_y = 1.89$ m for lateral undulation with gait parameters $\alpha = 35^o$, $\omega = 120^o/\text{s}$ and $\delta = 40^o$.

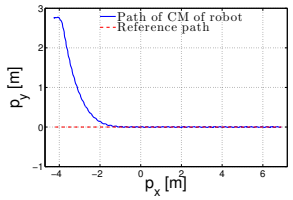

(a) Path of the CM

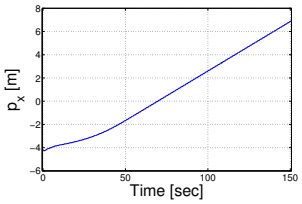

(b) Position along the path, p_x

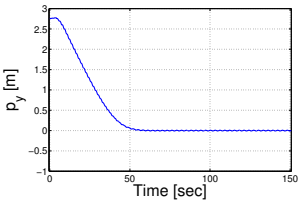

(c) Cross-track error, p_y

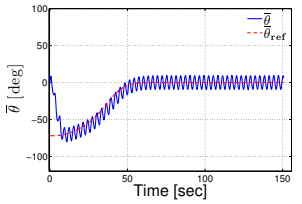

(d) Heading angle, $\overline{\theta}$

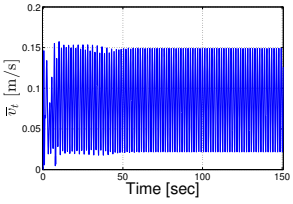

(e) Forward velocity, $\overline{v}_t$

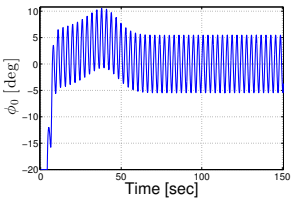

(f) Joint angle offset, ϕ_0

Fig. 19. Simulation results for straight line path following for a snake robot with $n = 9$ links initially headed along the desired path, and with the initial distance from the CM being $p_y = 2.75$ m for eel-like motion with gait parameters $\alpha = 40^o$, $\omega = 120^o/\text{s}$ and $\delta = 40^o$.

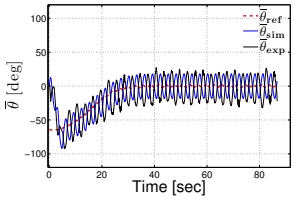

(a) Cross-track error, p_y

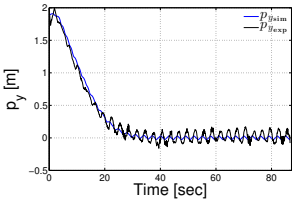

(b) Heading angle, $\bar{\theta}$

Fig. 20. Comparison results for straight line path following for a snake robot with $n = 9$ links initially headed along the desired path, and with the initial distance from the CM being $p_y = 2.75$ m for lateral undulation with gait parameters $\alpha = 35^o$, $\omega = 120^o/\text{s}$ and $\delta = 40^o$.

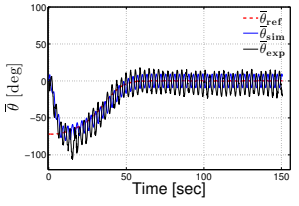

(a) Cross-track error, p_y

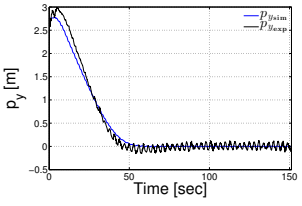

(b) Heading angle, $\bar{\theta}$

Fig. 21. Comparison results for straight line path following for a snake robot with $n = 9$ links initially headed along the desired path, and with the initial distance from the CM being $p_y = 2.75$ m for eel-like motion with gait parameters $\alpha = 40^o$, $\omega = 120^o/\text{s}$ and $\delta = 40^o$.

robot," in *Proc. MTS/IEEE International Conference Oceans*, vol. 1, Brest, France, June 20-23 2005, pp. 460–465.
[47] E. Kelasidi, K. Y. Pettersen, and J. T. Gravdahl, "Energy efficiency of underwater snake robot locomotion," in *Proc. 23th Mediterranean Conference on Control Automation (MED)*, Torremolinos, Spain, June 16-19 2015.
[48] ——, "Energy efficiency of underwater robots," in *Proc. 10th IFAC Conference on Manoeuvring and Control of Marine Craft (MCMC)*, Copenhagen, Denmark, Aug. 24-26 2015.
[49] ——, "Stability analysis of underwater snake robot locomotion based on averaging theory," in *Proc. IEEE International Conference on Robotics and Biomimetics (ROBIO)*, Bali, Indonesia, Dec. 5-10 2014, pp. 574–581.
[50] E. Kelasidi and A. Tzes, "Serpentine motion control of snake robots for curvature and heading based trajectory - parameterization," in *Proc. IEEE 20th Mediterranean Conference on Control Automation (MED)*, Barcelona, Spain, July 3-6 2012, pp. 536–541.
[51] E. Borhaug, A. Pavlov, and K. Pettersen, "Integral LOS control for path following of underactuated marine surface vessels in the presence of constant ocean currents," in *Proc. 47th IEEE Conference on Decision and Control (CDC)*, Cancun, Dec. 9-11 2008, pp. 4984–4991.
[52] E. Fredriksen and K. Y. Pettersen, "Global κ-exponential way-point maneuvering of ships: Theory and experiments," *Automatica*, vol. 42, no. 4, pp. 677 – 687, 2006.
[53] Marine cybernetics laboratory (MC-lab). [Online]. Available: http://www.ntnu.no/imt/lab/cybernetics
[54] Qualisys–motion capture systems. [Online]. Available: http://www.qualisys.com
[55] H.-P. Tan, R. Diamant, W. K. Seah, and M. Waldmeyer, "A survey of techniques and challenges in underwater localization," *Ocean Engineering*, vol. 38, no. 1415, pp. 1663 – 1676, 2011.
[56] J. Newman, *Marine Hydrodynamics*. MIT Press, 1977.
[57] P. Liljeback, K. Pettersen, O. Stavdahl, and J. Gravdahl, "Controllability and stability analysis of planar snake robot locomotion," *IEEE Transactions on Automatic Control*, vol. 56, no. 6, pp. 1365–1380, 2011.
[58] C. Jordan, "Coupling internal and external mechanics to predict swimming behavior: A general approach," *American Zoologist*, vol. 36, no. 6, pp. 710–722, 1996.

Eleni Kelasidi received the Diploma (MSc) of Electrical and Computer Engineering from the University of Patras, Greece, in 2009.

She is currently a PhD candidate in the Department of Engineering Cybernetics, Norwegian University of Science and Technology (NTNU). In 2009-2012, she was pre-doc researcher in the field of Design and Control of mobile robot with articulated body at the University of Patras. Her research interests include modeling, analysis and control of snake robots.

Pål Liljebäck received the M.Sc. and Ph.D. degrees in electrical engineering from the Norwegian University of Science and Technology (NTNU), Trondheim, Norway, in 2004 and 2011, respectively. He was a research scientist at SINTEF ICT, which is a Norwegian research organization, from 2004-2015. He is currently a Postdoctoral Researcher at the Department of Engineering Cybernetics, NTNU. He is first author of the book "Snake Robots: Modelling, Mechatronics, and Control" (Springer, 2013). His research interests include modeling and control of dynamical systems, and design and implementation of mechatronic systems.

Kristin Y. Pettersen is a Professor in the Department of Engineering Cybernetics, Norwegian University of Science and Technology (NTNU). She was Head of Department 2011-2013 and Director of the NTNU ICT Programme of Robotics 2010-2013. In 2013-2022 she is Key Scientist at the CoE Centre for Autonomous Marine Operations and Systems (AMOS). She received the MSc and PhD degrees in Engineering Cybernetics at NTH/NTNU in 1992 and 1996. She has published 200 papers for conferences and journals, and her research interests focus on nonlinear control of mechanical systems, with a special emphasis on marine robotics and snake robotics. She has co-edited the Springer Verlag book "Group Coordination and Cooperative control", and is co-author of the Springer Verlag books "Snake Robots" and "Modeling and Control of Vehicle-Manipulator Systems". She is an Associate Editor of the IEEE Transactions on Control Systems Technology and the IEEE Control Systems Magazine. She was a member of the Board of Governors of IEEE Control Systems Society 2012-2014.
Prof. Pettersen received the IEEE Transactions on Control Systems Technology outstanding paper award in 2006.

Jan Tommy Gravdahl received the Siv.ing and Dr.ing degrees in engineering cybernetics from the Norwegian University of Science and Technology (NTNU), Trondheim, Norway, in 1994 and 1998, respectively.

He became an Associate Professor in 2001 and then Professor in 2005 in the Department of Engineering Cybernetics, NTNU, where he also served as the Head of the Department in 2008-2009. In 2007-2008, he was a Visiting Professor at the Centre for Complex Dynamic Systems and Control, The University of Newcastle, Newcastle, Australia. He has published more than 150 international conference and journal papers. He is the author of Compressor Surge and Rotating Stall: Modeling and Control (Springer, 1999), coauthor of Modeling and Simulation for Automatic Control (Marine Cybernetics, 2002), coeditor of Group Coordination and Cooperative Control (Springer, 2006), and coauthor of Snake Robots: Modelling, Mechatronics, and Control (Springer, 2013). He is also a coauthor of Modeling and Control of Vehicle-Manipulator Systems (Springer, 2013). His current research interests include mathematical modeling and nonlinear control in general, modeling and control of turbomachinery, and control of vehicles, spacecraft, robots, and nanopositioning devices.
Prof. Gravdahl received the IEEE TRANSACTIONS ON CONTROL SYSTEMS TECHNOLOGY Outstanding Paper Award in 2000.